

# ONLINE MULTISCALE MODEL REDUCTION FOR NONLINEAR STOCHASTIC PDES WITH MULTIPLICATIVE NOISE \*

LIJIAN JIANG<sup>1†</sup>, MENGANAN LI<sup>1‡</sup>, AND MENG ZHAO<sup>1§</sup>

**Abstract.** In this paper, an online multiscale model reduction method is presented for stochastic partial differential equations (SPDEs) with multiplicative noise, where the diffusion coefficient is spatially multiscale and the noise perturbation nonlinearly depends on the diffusion dynamics. It is necessary to efficiently compute all possible trajectories of the stochastic dynamics for quantifying model's uncertainty and statistic moments. The multiscale diffusion and nonlinearity may cause the computation very intractable. To overcome the multiscale difficulty, a constraint energy minimizing generalized multiscale finite element method (CEM-GMsFEM) is used to localize the computation and obtain an effective coarse model. However, the nonlinear terms are still defined on a fine scale space after the Galerkin projection of CEM-GMsFEM is applied to the nonlinear SPDEs. This significantly impacts on the simulation efficiency by CEM-GMsFEM. To this end, a stochastic online discrete empirical interpolation method (DEIM) is proposed to treat the stochastic nonlinearity. The stochastic online DEIM incorporates offline snapshots and online snapshots. The offline snapshots consist of the nonlinear terms at the approximate mean of the stochastic dynamics and are used to construct an offline reduced model. The online snapshots contain some information of the current new trajectory and are used to correct the offline reduced model in an increment manner. The stochastic online DEIM substantially reduces the dimension of the nonlinear dynamics and enhances the prediction accuracy for the reduced model. Thus, the online multiscale model reduction is constructed by using CEM-GMsFEM and the stochastic online DEIM. A priori error analysis is carried out for the nonlinear SPDEs. We present a few numerical examples with diffusion in heterogeneous porous media and show the effectiveness of the proposed model reduction.

**Key words.** nonlinear stochastic PDEs, multiscale model reduction, online DEIM

**1. Introduction.** Fluid flow in porous media has been an active and attractive research field for the last several decades. Contamination of groundwater, underground oil flow in the petroleum industry and blood flow through capillaries are the relevant porous media applications. The study of flows in porous media is of significant importance for ecology, industry, biology, etc. These problems typically involves multiple spatial and temporal scales. Multiscale coefficients in these models are often used to describe the porosity, permeability, diffusion process and so on. The deterministic multiscale models have been thoroughly studied in lot of literatures [4, 18, 24, 28, 34, 39] and reference therein.

However, many natural phenomena in porous media exhibit inherent randomness, such as the permeability of porous media varying in an irregular manner [35]. These phenomena can not be modeled with deterministic PDEs. Therefore, more sophisticated theories and concepts are needed to take account of the complex behavior of these systems. Stochastic partial differential equations (SPDEs) can model those natural systems in a comprehensive manner. Stochastic models in porous media [5, 6, 27] are studied much less than the deterministic systems, while this kind of stochastic situations abound in real-world applications. In this paper, we consider stochastic parabolic partial differential models in highly heterogeneous porous me-

---

\*L.Jiang acknowledges the support of NSFC 11871378, the Fundamental Research Funds for the Central Universities and the support by Shanghai Science and Technology Committee 20JC1413500.

<sup>†</sup>School of Mathematical Sciences, Tongji University, Shanghai 200092, China. (ljjiang@tongji.edu.cn).

<sup>‡</sup>School of Mathematics, Hunan University, Changsha 410082, China. (mengnanli@hnu.edu.cn).

<sup>§</sup>School of Mathematical Sciences, Tongji University, Shanghai 200092, China. (1910736@tongji.edu.cn).

media with inherent multiple scales. When the coefficients of noise are relevant with the solution itself, these equations are called SPDEs driven by multiplicative noise, while the noise perturbation, independent of solution, corresponds to additive noise. SPDEs with multiplicative noise are usually more complicated than SPDEs with additive noise. Moreover, nonlinearity of the noise perturbation may result in a significant challenge for simulating dynamical systems. To this end, we develop a model reduction to take care of multiple scales and nonlinearity of SPDEs in porous media.

Many multiscale methods have been developed to effectively compute multiscale models in the past few years, such as multiscale finite element methods (MsFEM) [8, 17], multiscale finite volume method [23], heterogeneous multiscale methods [15], mixed multiscale finite element methods [1, 2, 11], variational multiscale methods [20, 21, 22], mortar multiscale methods [3, 41], and generalized multiscale finite element method (GMsFEM) [9, 16], localization orthogonal decomposition [32], constraint energy minimizing generalized multiscale finite element method (CEM-GMsFEM) [10, 29].

In the paper, we use CEM-GMsFEM to solve multiscale SPDEs. The construction of CEM-GMsFEM basis functions is usually divided into two stages. Firstly, we solve a local eigenproblem to get a set of auxiliary basis functions on each coarse block. Secondly, we solve a constraint energy minimization problem, where the constraints are involved with auxiliary basis functions. When CEM-GMsFEM is applied to nonlinear problems, the discretization system is still nonlinear and is defined in a fine grid space. The evaluation of the nonlinear terms, as well as computation of the residual and the Jacobian matrix, are still all required on the fine grid, when we derive the full discretization scheme by a stable temporal implicit method. Moreover, nonlinearity may lead to a slow convergence for iteration methods (e.g., Newton method) to solve the nonlinear problems in a high dimensional space. Thus, the nonlinearity may bring a significant computation challenge for solving nonlinear multiscale SPDEs.

We focus on the nonlinear systems stemming from the spatial discretization using CEM-GMsFEM and seek an effective model reduction method to improve the computation efficiency. Proper orthogonal decomposition (POD) is one of popular model reduction methods and constructs a set of basis vectors with solution snapshots. These basis vectors span a low-dimensional reduced space which the full-order system is projected onto. But POD still needs the evaluation of nonlinear functions at all states, which makes solving the reduced system as computationally expensive as solving the original high-dimensional problem. Thus POD is not appropriate to straightforwardly treat the nonlinear problems. To overcome the drawback of POD, the discrete version of the empirical interpolation method [7], DEIM [12, 13, 36] has been proposed to effectively reduce the computation complexity of nonlinear problems.

Typically, DEIM includes two phases. The first phase is the offline phase where a reduced system is constructed using the solution of full-order system. The second phase is the online phase in which we apply the precomputed reduced system to approximate the solution of new problem at hand. The offline phase computes the basis matrix and interpolation matrix by applying POD to a set of nonlinear snapshots, while the online phase uses the obtained matrixes to interpolate online nonlinear functions in a low dimension space. The traditional DEIM works well for deterministic nonlinear systems, but it may be not sufficient for stochastic dynamical systems. The solution of SPDE is a stochastic process, which includes all trajectories corresponding to different samples of noise. If we apply DEIM to the mean of snapshots associated

with trajectories in the offline phase and adopt the reduced system for any new trajectory of solution, there may exist a large error because the precomputed reduced system does not contain any information from the new trajectory. Of course, one can implement DEIM individually for each new trajectory. But it costs much online computation and is not suitable for the many-query applications such as uncertainty quantification and the computation of statistics. To this end, we propose a stochastic online DEIM to reduce the stochastic models. The proposed online DEIM also includes two phases: offline phase and online phase. In the offline phase, we utilize a sort of mean information of nonlinear functions as the snapshots, and adopt DEIM to construct the offline basis matrix and interpolation matrix. In the online phase, the newly generated data ( evaluation of the nonlinear functions along the new trajectory) is used to update the offline basis matrix in an increment manner. The stochastic online DEIM incorporates the precomputed model (mean of old trajectories) and the new trajectory information into the model reduction. This approach can improve the fitness and prediction of the reduced model. A multiscale stochastic model reduction for SPDEs is constructed by combining CEM-GMsFEM with stochastic online DEIM, and is referred to as Online DEIM-MS in the paper.

This article is organized as follows. Section 2 is to introduce some preliminary knowledge of SPDEs and weak formulations. In Section 3, we present CEM-GMsFE for SPDEs and give a priori error analysis for nonlinear SPDEs with multiplicative noise. The stochastic online DEIM is addressed in Section 4. In Section 5, a few numerical examples in porous media are presented to show the applicability and effectiveness of Online DEIM-MS. Some conclusions are made finally.

**2. Preliminaries.** Let  $D$  be a bounded spatial domain in  $\mathbb{R}^d$  ( $d = 2$ ),  $T > 0$  a fixed time,  $H := L^2(D)$  a Hilbert space with norm  $\|\cdot\|_H$ . In this work, we consider the following nonlinear stochastic partial differential problem: find a  $H$ -valued stochastic process  $u(t)$  to solve the SPDE with a multiplicative noise

$$\begin{cases} du - \nabla \cdot (\kappa(x)\nabla u)dt = f(u)dt + g(u)dW(t) & \text{in } D \times (0, T], \\ u(x, t) = 0 & \text{on } \partial D \times (0, T], \\ u(x, 0) = u_0(x) & \text{in } D, \end{cases} \quad (2.1)$$

or formally

$$\begin{cases} u_t - \nabla \cdot (\kappa(x)\nabla u) = f(u) + g(u)\xi(t) & \text{in } D \times (0, T], \\ u(x, t) = 0 & \text{on } \partial D \times (0, T], \\ u(x, 0) = u_0(x) & \text{in } D, \end{cases} \quad (2.2)$$

where  $u_0(x)$  is the initial condition,  $\kappa(x)$  is a multiscale diffusion coefficient,  $f$  and  $g$  are  $H$ -valued nonlinear functionals,  $W(t)$  is a  $H$ -valued  $\mathcal{Q}$ -Wiener process defined in a filtered probability space  $(\Omega, \mathcal{F}, \mathbb{P}, \{\mathcal{F}_t\}_{t \geq 0})$  [35], and  $\xi := \frac{dW}{dt}$  is  $H$ -valued noise. The filtered probability space is assumed to fulfill the usual conditions [37]. In the triple  $(\Omega, \mathcal{F}, \mathbb{P})$ ,  $\Omega$  is the sample space,  $\mathcal{F}$  is the  $\sigma$ -algebra of subset of  $\Omega$ , and a probability measure  $\mathbb{P}$  on  $(\Omega, \mathcal{F})$  is a function  $\mathbb{P} : \mathcal{F} \rightarrow [0, 1]$ .  $\kappa(x)$  refers to permeability and is often heterogeneous in practical models. In this paper, we follow the conventional notation, and suppress the dependence on space and write  $u(t)$  for  $u(t, x)$  and  $W(t)$  for  $W(t, x)$ . Equation (2.1) can be viewed as a mathematical model for the dynamics of diffusion-reaction flows driven by the stochastic perturbation  $g(u)dW(t)$  in natural formations such as aquifers. In the modeling of solute transport problem in porous

media,  $u$  represents the solute concentration, while the dispersion of the solute is primarily affected by the spatial heterogeneity or porosity [27].

We assume that the covariance operator  $\mathcal{Q} : H \rightarrow H$  is non-negative, symmetric and of trace class, i.e., the series  $Tr(\mathcal{Q}) := \sum_{i \in \mathbb{N}} (\mathcal{Q}\eta_i, \eta_i)_H$  converges, where  $\{\eta_i\}_{i \in \mathbb{N}}$  is an arbitrary orthonormal basis of  $H$ , and  $Tr(\mathcal{Q}) < \infty$ . Then the  $\mathcal{Q}$ -Wiener process [19, 30]  $W(t)$  can be represented as

$$W(t) = \sum_{i \in \mathbb{N}} \sqrt{\mu_i} e_i \beta_i(t), \quad t \in [0, T], \quad (2.3)$$

where  $\mu_i \geq 0$ ,  $e_i$  ( $i \in \mathbb{N}$ ) are respectively the eigenvalues and the eigenfunctions of the covariance operator  $\mathcal{Q}$  in  $H$ , and  $\beta_i(t)$  are independent and identically distributed standard  $\mathcal{F}_t$ -Brownian motions.

For analysis, we review some basic properties about the stochastic Itô integral for integrable stochastic process with respect to  $\mathcal{Q}$ -Wiener process. Let  $L_2^0 := HS(\mathcal{Q}^{1/2}H, H)$  be the space of Hilbert-Schmidt operators from  $\mathcal{Q}^{1/2}H$  to  $H$ , endowed with  $\|\cdot\|_{L_2^0}$  norm, which is defined by

$$\|\phi\|_{L_2^0} := \|\phi\mathcal{Q}^{1/2}\|_{HS} = \left( \sum_{i=1}^{\infty} \|\phi\mathcal{Q}^{1/2}\eta_i\|_H^2 \right)^{1/2}, \quad \forall \phi \in L_2^0,$$

where  $\{\eta_i\}_{i=1}^{\infty}$  is an orthonormal basis in  $H$ . The space  $L_2^0$  is separable. We refer to [19, 25, 37] for the detailed introduction to these definitions. In this paper, we assume that the integrability of all  $L_2^0$ -valued stochastic processes is satisfied.

**PROPOSITION 2.1.** [37] (*Martingale*) For any  $L_2^0$ -valued integrable stochastic process  $\phi$ , the stochastic process

$$M(t) := \int_0^t \phi dW(\tau) = 0, \quad t \in [0, T],$$

is a continuous, square integrable martingale with

$$\mathbf{E}[M(t)] = 0. \quad (2.4)$$

**PROPOSITION 2.2.** [37] (*Itô isometry*) For any  $L_2^0$ -valued integrable stochastic process  $\phi$ ,

$$\mathbf{E} \left\| \int_0^t \phi dW(s) \right\|^2 = \mathbf{E} \int_0^t \|\phi\|_{L_2^0}^2 ds. \quad (2.5)$$

Suppose that the coefficient  $\kappa(x)$  is uniformly positive and bound in  $\Omega$ , i.e., there exists  $0 < \kappa_0 < \kappa_1 < \infty$  such that  $\kappa_0 \leq \kappa(x) \leq \kappa_1$ , but the ratio  $\kappa_1/\kappa_0$  can be large. Let operator  $\mathcal{A} := -\nabla \cdot (\kappa(x)\nabla \cdot)$  and space

$$\mathcal{H} := L^2(\Omega, L^2(D \times [0, T]))$$

equipped with norm  $\|\cdot\|_{\mathcal{H}}$ . We make the following assumptions to ensure a unique mild solution of the equation (2.1) or (2.2).

A.1  $f : H \rightarrow H$  is globally Lipschitz continuous and of linear growth, i.e.,

$$\begin{aligned} \|f(u) - f(v)\|_H &\leq L_f \|u - v\|_H, \\ \|f(w)\|_H &\leq C_f(1 + \|w\|_H), \quad \forall u, v, w \in H. \end{aligned} \quad (2.6)$$

Here  $f$  is the so-called Nemytskii operator defined for  $H$ .

A.2  $g : H \rightarrow L_0^2$  is also globally Lipschitz continuous and of linear growth, i.e.,

$$\begin{aligned} \|g(u) - g(v)\|_{L_0^2} &\leq L_g \|u - v\|_H, \\ \|g(w)\|_{L_0^2} &\leq C_g(1 + \|w\|_H), \quad \forall u, v, w \in H. \end{aligned} \quad (2.7)$$

A.3  $u_0 \in L^2(\Omega, L^2(\mathcal{D}(-\mathcal{A})^{1/2}))$  is measurable, i.e.,  $\mathbf{E} \|\nabla u_0\|^2 < +\infty$ .

**THEOREM 2.3.** [38] *Assume that A.1-A.3 hold. Then the equation (2.1) or (2.2) admits unique mild solution in the form*

$$u(t) = E(t)u_0 + \int_0^t E(t-s)f(u(s))ds + \int_0^t E(t-s)g(u(s))dW(s), \quad t \in [0, T], \quad (2.8)$$

where  $E(t) := e^{-t\mathcal{A}}, t \geq 0$ , is an analytic semigroup of the linear operator  $-\mathcal{A}$ , such that  $\sup_{t \in [0, T]} \mathbf{E} \|u(t)\|_H^2 < +\infty$ .

By Theorem 9.15 in [38], the existence and uniqueness of the mild solution is equivalent to the existence and uniqueness of the weak solution under the assumptions A.1-A.3, i.e., there exists a unique weak solution  $u(\cdot, t, \omega) \in H$  such that  $\sup_{t \in [0, T]} \mathbf{E} \|u(t)\|_H^2 < +\infty$ , and for  $\forall v \in H_0^1, t \in [0, T]$ , we have

$$(u(t), v) = (u_0, v) - \int_0^t (\kappa(x)\nabla u(s), \nabla v)ds + \int_0^t (f(u(s)), v)ds + \int_0^t (g(u(s))dW(s), v), \quad (2.9)$$

where

$$\int_0^t (g(u(s))dW(s), v) := \sum_{i=1}^{\infty} \int_0^t (g(u(s))\sqrt{\mu_i}e_i, v)d\beta_i(s).$$

Thus we get the variational form of (2.2),

$$\begin{cases} (u_t, v) + a(u, v) = (f(u), v) + (g(u)\xi(t), v) & \forall v \in H_0^1, t > 0, \\ (u(\cdot, 0), v) = (u_0, v) & \forall v \in H_0^1, \end{cases} \quad (2.10)$$

where

$$a(u, v) = (\kappa\nabla u, \nabla v) = \int_D \kappa\nabla u \cdot \nabla v, \quad (f, v) = \int_D fv.$$

The first aim of this paper is to carry out a CEM-MsFE convergence analysis for the equation (2.1). To this end, we construct a multiscale finite element space  $V_{ms} \subset H_0^1$ . The CEM-GMsFE solution  $u(\cdot, t) \in V_{ms}$  solves

$$\begin{cases} ((u_{ms})_t, v) + a(u_{ms}, v) = (f(u_{ms}), v) + (g(u_{ms})\xi(t), v) & \forall v \in V_{ms}, t > 0, \\ (u_{ms}(\cdot, 0), v) = (u_{0,ms}, v) & \forall v \in V_{ms}, \end{cases} \quad (2.11)$$

where  $u_{0,ms} \in V_{ms}$  is the  $L^2$  projection of  $u_0$  onto  $V_{ms}$ .

**3. CEM-GMsFE method for SPDE.** In this section, we first present the construction for multiscale basis functions. Then a priori error analysis is carried out for the SPDE (2.1) in CEM-GMsFEM.

**3.1. Construction of multiscale basis functions.** This subsection will follow the works [9, 10, 16, 29], and focus on the construction of the CEM-GMsFEM basis functions for the equation (2.1). The multiscale finite element space is constructed by solving constrained energy minimization problems.

Let  $\mathcal{T}_h$  be a coarse grid partition of the space domain  $\Omega$  with  $N_c$  nodes,  $N$  elements, and  $h$  the size of a generic coarse element. Figure 3.1 shows the fine grid, the coarse grid  $K_i$  and oversampling domain  $K_i^m$  by enlarging coarse layers ( $m = 2$ ).

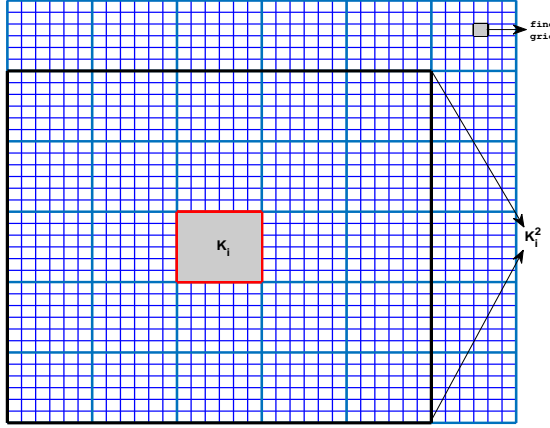


FIG. 3.1. The fine grid, coarse grid  $K_i$ , oversampling domain  $K_i^2$

For each coarse block  $K_i \in \mathcal{T}_h$ , we denote  $V(K_i) := H^1(K_i)$ , and consider a set of auxiliary basis functions  $\{\phi_j^{(i)}\}_{j=1}^{L_i} \in V(K_i)$  by solving the spectral problem

$$a_i(\phi_j^{(i)}, v) = \lambda_j^{(i)} s_i(\phi_j^{(i)}, v), \quad \forall v \in V(K_i), \quad (3.1)$$

where  $s_i(\phi_j^{(i)}, v) = \int_{K_i} \tilde{\kappa} uv$ , and  $\tilde{\kappa} = \kappa \sum_i |\Delta \chi_i|^2$ ,  $\{\chi_i\}$  is a set of partition of unity functions for the coarse partition. We collect the first  $L_i$  eigenfunctions corresponding to the first  $L_i$  smallest eigenvalues for the local auxiliary multiscale space  $V_{aux}^{(i)} = \text{span}\{\phi_j^{(i)} | 1 \leq j \leq L_i\}$  and define the global auxiliary space  $V_{aux}$  by the direct sum of these local spaces,

$$V_{aux} = \bigoplus_{i=1}^N V_{aux}^{(i)}.$$

Let the oversampling domain  $K_i^m \subset \Omega$  be the extension of  $K_i$  with  $m$  coarse grid layers (as in Figure 3.1). The CEM-MsFE basis functions  $\varphi_{j,ms}^{(i)} \in H_0^1(K_i^m)$  are constructed

through solving the local problems

$$\varphi_{j,ms}^{(i)} = \arg \min \left\{ a(\varphi, \varphi) \mid \varphi \in H_0^1(K_i^m), \varphi \text{ is } \phi_j^{(i)}\text{-orthogonal} \right\}, \quad (3.2)$$

where  $\varphi \in V$  is  $\phi_j^{(i)}$ -orthogonal when

$$s(\varphi, \phi_j^{(i)}) = 1 \quad \text{and} \quad s(\varphi, \phi_{j'}^{(i')}) = 0, \quad \text{if } j' \neq j \text{ or } i' \neq i,$$

with  $s(u, v) = \sum_{i=1}^N s_i(u, v)$ . Thus, we define the multiscale finite element space for CEM-GMsFEM by

$$V_{ms} = \text{span} \left\{ \varphi_{j,ms}^{(i)} \mid 1 \leq j \leq L_i, 1 \leq i \leq N \right\}.$$

**REMARK 3.1.** *Lemma 5 in [10] implies that more layers  $m$  of the oversampling domain  $K_i^m$  can improve the approximation accuracy of the multiscale method. But the multiscale basis functions decay to zero on the oversampling domain as more layers are utilized [10, 29]. Thus, we may use a small number of layers for the oversampling domain to balance the approximation accuracy and computation efficiency.*

**3.2. A priori error analysis.** In this subsection, we approximate the solution  $u(x, t)$  of the problem (2.10) by a function  $u_{ms} \in V_{ms}$  for each  $t > 0$ . First of all, we provide the error estimates of CEM-GMsFEM for the SPDE with multiplicative noise. To this end, we need some preliminary lemmas.

**LEMMA 3.1.** *Let  $u$  be the solution of the stochastic parabolic equation (2.1). Then*

$$\mathbf{E} \|u_t\|_{L^2(D \times [0, T])}^2 \leq C \left( \mathbf{E} \|u_0\|_a^2 + \|f(u)\|_{\mathcal{H}}^2 \right), \quad (3.3)$$

where  $\|u\|_a^2 := \int_D \kappa |\nabla u|^2$  is the energy norm.

*Proof.* By (2.10), we have

$$(u_t, u_t) + a(u, u_t) = (f(u), u_t) + (g(u)\xi(t), u_t),$$

which implies

$$\|u_t\|_H^2 + \frac{1}{2} \frac{d}{dt} \|u\|_a^2 = (f(u), u_t) + (g(u)\xi(t), u_t).$$

Integrating over the interval  $[0, t]$ ,  $0 \leq t \leq T$  and taking the expectation of both sides, we get

$$\begin{aligned} & \mathbf{E} \int_0^t \|u_t(x, s)\|_H^2 ds + \frac{1}{2} \mathbf{E} \|u(x, t)\|_a^2 \\ &= \mathbf{E} \int_0^t (f(u), u_t) ds + \mathbf{E} \int_0^t (g(u)\xi(s), u_t) ds + \frac{1}{2} \mathbf{E} \|u_0\|_a^2 \\ &= \mathbf{E} \int_0^t (f(u), u_t) ds + \mathbf{E} \int_0^t (g(u) dW(s), u_t) + \frac{1}{2} \mathbf{E} \|u_0\|_a^2 \\ &\leq \mathbf{E} \int_0^t \frac{1}{2} (\|f(u)\|_H^2 + \|u_t\|_H^2) ds + \frac{1}{2} \mathbf{E} \|u_0\|_a^2, \end{aligned}$$

where  $\mathbf{E} \int_0^t (g(u(s))dW(s), u_t) = 0$  has been used in the third step by Prop.2.1. This completes the proof.  $\square$

REMARK 3.2. Since  $f(u)$  is of linear growth and a Nemytskii operator in  $H$  and the weak solution of (2.2)  $u \in L^\infty([0, T], L^2(D \times \Omega))$ , i.e.,  $\|f(u)\|_H \leq C_f(1 + \|u\|_H)$ ,  $\forall u \in H$  and  $\sup_{t \in [0, T]} \mathbf{E} \|u(t)\|_H^2 < +\infty$ , then further we have the following estimation by Lemma 3.1,

$$\begin{aligned} \mathbf{E} \|u_t\|_{L^2(D \times [0, T])}^2 &\leq C \left( \mathbf{E} \|u_0\|_a^2 + \|f(u)\|_{\mathcal{H}}^2 \right) \\ &\leq C \left( \mathbf{E} \|u_0\|_a^2 + 2C_f(1 + \|u\|_{\mathcal{H}}^2) \right) \\ &\leq C \left( \mathbf{E} \|u_0\|_a^2 + 2C_f \left( 1 + \|u\|_{L^\infty([0, T], L^2(D \times \Omega))}^2 \right) \right) \\ &< +\infty. \end{aligned}$$

Let  $\widehat{u} \in V_{ms}$  be the elliptic projection of the function  $u \in V$ , i.e.,  $\widehat{u}$  satisfies

$$a(\widehat{u}, v) = a(u, v), \quad \forall v \in V_{ms}.$$

From Lemma 3.1, we immediately have the following estimates of  $\widehat{u}$  and  $u_{ms}$ , respectively,

$$\begin{aligned} \mathbf{E} \|\widehat{u}_t\|_{L^2(D \times [0, T])}^2 &\leq C \left( \mathbf{E} \|\widehat{u}_0\|_a^2 + \|f(u)\|_{\mathcal{H}}^2 \right), \\ \mathbf{E} \|(u_{ms})_t\|_{L^2(D \times [0, T])}^2 &\leq C \left( \mathbf{E} \|u_{0,ms}\|_a^2 + \|f(u)\|_{\mathcal{H}}^2 \right). \end{aligned} \quad (3.4)$$

By Lemma 4.3 in [29], we have the following estimate between the solution of stochastic parabolic equation and its corresponding elliptic projection.

LEMMA 3.2. Let  $u$  be the solution of (2.1). For each  $t > 0$ , any fixed realization  $\xi(t)$ , the elliptic projection  $\widehat{u}(t) \in V_{ms}$  and satisfies

$$a(u(t) - \widehat{u}(t), v) = 0, \quad \forall v \in V_{ms}. \quad (3.5)$$

Then, for any  $t > 0$ ,

$$\begin{aligned} \|(u - \widehat{u})(t)\|_a &\leq Ch\Lambda^{-\frac{1}{2}} \|\kappa^{-\frac{1}{2}}(f(u) + g(u)\xi(t) - u_t)(t)\|_H, \\ \|(u - \widehat{u})(t)\|_H &\leq Ch^2\Lambda^{-1}\kappa_0^{-\frac{1}{2}} \|\kappa^{-\frac{1}{2}}(f(u) + g(u)\xi(t) - u_t)(t)\|_H, \end{aligned}$$

where  $C$  is a constant independent of  $\kappa$  and the mesh size  $h$ , and  $\Lambda = \min_{1 \leq i \leq N} \lambda_{L_i+1}^{(i)}$  is the smallest eigenvalue that we discard when constructing the local auxiliary multiscale space.

REMARK 3.3. By Lemma 3.2 and Lemma 3.1, assuming  $g(u)\xi(t) \in \mathcal{H}$ , we further have the following estimations,

$$\mathbf{E} \int_0^t \|(u - \widehat{u})(s)\|_a^2 ds \leq Ch^2\Lambda^{-1}\kappa_0^{-1} (\|f(u)\|_{\mathcal{H}}^2 + \|g(u)\xi(t)\|_{\mathcal{H}}^2 + \mathbf{E} \|u_0\|_a^2), \quad (3.6)$$

$$\mathbf{E} \int_0^t \|(u - \widehat{u})(s)\|_H^2 ds \leq Ch^4\Lambda^{-2}\kappa_0^{-2} (\|f(u)\|_{\mathcal{H}}^2 + \|g(u)\xi(t)\|_{\mathcal{H}}^2 + \mathbf{E} \|u_0\|_a^2). \quad (3.7)$$



In the following theorem, we prove a strong convergence of the semidiscrete solution of (2.11).

**THEOREM 3.3.** *Let  $u$  and  $u_{ms}$  be the solution of (2.10) and (2.11), respectively. Then for any fixed  $t \in [0, T]$ ,*

$$\begin{aligned} & \mathbf{E} \|(u - u_{ms})(t)\|_H^2 + \mathbf{E} \int_0^t \|u - u_{ms}\|_a^2 ds \\ & \leq Ch^2 \Lambda^{-1} \kappa_0^{-1} (\|f(u)\|_{\mathcal{H}}^2 + \|g(u)\xi(x, t)\|_{\mathcal{H}}^2 + \mathbf{E} \|u_0\|_a^2 + \mathbf{E} \|u_{0,ms}\|_a^2) \\ & + \mathbf{E} \|(u - u_{ms})(0)\|_H^2, \end{aligned} \quad (3.8)$$

where  $C$  is a constant independent of  $\kappa$  and the mesh size  $h$ .

*Proof.* By (2.10) and (2.11), we have

$$(u_t, v) + a(u, v) = (f(u), v) + (g(u)\xi(t), v), \quad (3.9)$$

$$((u_{ms})_t, v) + a(u_{ms}, v) = (f(u_{ms}), v) + (g(u_{ms})\xi(t), v) \quad (3.10)$$

for all  $v \in V_{ms}$ . Thus, by subtracting (3.10) from (3.9), we get, for  $\forall v \in V_{ms}$

$$((u - u_{ms})_t, v) + a(u - u_{ms}, v) = (f(u) - f(u_{ms}), v) + (g(u)\xi - g(u_{ms})\xi, v). \quad (3.11)$$

The elliptic projection of  $u$ ,  $\hat{u} \in V_{ms}$ , satisfies (3.6) and (3.7). In particular, by taking  $v = \hat{u} - u_{ms} \in V_{ms}$  in (3.11), we have the following error equation,

$$\begin{aligned} & ((u - u_{ms})_t, \hat{u} - u_{ms}) + a(u - u_{ms}, \hat{u} - u_{ms}) \\ & = (f(u) - f(u_{ms}), \hat{u} - u_{ms}) + ((g(u) - g(u_{ms}))\xi, \hat{u} - u_{ms}). \end{aligned} \quad (3.12)$$

Due to the bilinearity of  $a(\cdot, \cdot)$ , we can rewrite (3.12) as

$$\begin{aligned} & ((u - u_{ms})_t, u - u_{ms}) + a(u - u_{ms}, u - u_{ms}) \\ & + (f(u_{ms}) - f(u), u - u_{ms}) + ((g(u_{ms}) - g(u))\xi, u - u_{ms}) \\ & = ((u - u_{ms})_t, u - \hat{u}) + a(u - u_{ms}, u - \hat{u}) \\ & + (f(u_{ms}) - f(u), u - \hat{u}) + ((g(u_{ms}) - g(u))\xi, u - \hat{u}). \end{aligned}$$

The Lipschitz assumptions of  $f$ , Cauchy-Schwarz inequality and Young's inequality give

$$\begin{aligned} & \frac{1}{2} \frac{d}{dt} \|u - u_{ms}\|^2 + \|u - u_{ms}\|_a^2 - L_f \|u - u_{ms}\|^2 + ((g(u_{ms}) - g(u))\xi, u - u_{ms}) \\ & \leq ((u - u_{ms})_t, u - \hat{u}) + a(u - u_{ms}, u - \hat{u}) + \frac{1}{2} L_f \|u - u_{ms}\|^2 + \frac{1}{2} \|u - \hat{u}\|^2 \\ & + ((g(u_{ms}) - g(u))\xi, u - \hat{u}). \end{aligned}$$

After taking integration over  $[0, t]$  for  $\forall t, 0 \leq t \leq T$ , and taking expectation with respect to random process, and using the Cauchy-Schwarz and Young's inequalities

to the right-hand side, it follows that

$$\begin{aligned}
& \mathbf{E} \|(u - u_{ms})(t)\|_H^2 + \mathbf{E} \int_0^t \|u - u_{ms}\|_a^2 ds \\
& \leq 2\mathbf{E} \int_0^t (\|u_t\|_H + \|(u_{ms})_t\|_H) \|u - \widehat{u}\|_H ds + \mathbf{E} \int_0^t \|u - \widehat{u}\|_a^2 ds + \mathbf{E} \int_0^t \|u - \widehat{u}\|_H^2 ds \\
& + 3L_f \mathbf{E} \int_0^t \|u - u_{ms}\|_H^2 ds + \mathbf{E} \|(u - u_{ms})(0)\|_H^2,
\end{aligned} \tag{3.13}$$

where we used the following result by Prop.2.1,

$$\begin{aligned}
\mathbf{E} \int_0^t \left( (g(u_{ms}) - g(u))\xi(s), u - u_{ms} \right) ds &= \mathbf{E} \int_0^t \left( (g(u_{ms}) - g(u))dW(s), u - u_{ms} \right), \\
\mathbf{E} \int_0^t \left( (g(u_{ms}) - g(u))\xi(s), u - \widehat{u} \right) ds &= \mathbf{E} \int_0^t \left( (g(u_{ms}) - g(u))dW(s), u - \widehat{u} \right).
\end{aligned}$$

For the first term on the right-hand side of (3.13), Hölder inequality implies

$$\begin{aligned}
& \mathbf{E} \int_0^t (\|u_t\|_H + \|(u_{ms})_t\|_H) \|u - \widehat{u}\|_H ds \\
& \leq \mathbf{E} \left\{ \left( \int_0^t (\|u_t\|_H + \|(u_{ms})_t\|_H)^2 ds \right)^{\frac{1}{2}} \left( \int_0^t \|u - \widehat{u}\|_H^2 ds \right)^{\frac{1}{2}} \right\}.
\end{aligned} \tag{3.14}$$

For presentation convenience, we define

$$\begin{aligned}
I &:= 2\mathbf{E} \left\{ \left( \int_0^t (\|u_t\|_H + \|(u_{ms})_t\|_H)^2 ds \right)^{\frac{1}{2}} \left( \int_0^t \|u - \widehat{u}\|_H^2 ds \right)^{\frac{1}{2}} \right\} \\
& + \mathbf{E} \int_0^t \|u - \widehat{u}\|_a^2 ds + \mathbf{E} \int_0^t \|u - \widehat{u}\|_H^2 ds + \mathbf{E} \|(u - u_{ms})(0)\|_H^2.
\end{aligned} \tag{3.15}$$

Hence, from (3.13), (3.14) and (3.15), we get

$$\begin{aligned}
\mathbf{E} \|(u - u_{ms})(t)\|_H^2 + \mathbf{E} \int_0^t \|u - u_{ms}\|_a^2 ds &\leq I + 3L_f \mathbf{E} \int_0^t \|u - u_{ms}\|_H^2 ds \\
&\leq I + 3L_f \mathbf{E} \int_0^t \left( \|u - u_{ms}\|_H^2 + \int_0^t \|u - u_{ms}\|_a^2 d\tau \right) ds.
\end{aligned}$$

The Gronwall inequality concludes that

$$\mathbf{E} \|(u - u_{ms})(t)\|_H^2 + \mathbf{E} \int_0^t \|u - u_{ms}\|_a^2 ds \leq CI. \tag{3.16}$$

Finally, combining Lemma 3.1, Corollary 3.4, Lemma 3.2, Remark 3.3 and (3.16), we complete the proof.  $\square$

In particular, for stochastic parabolic PDEs with additive noise, which is the degeneration of (2.1), i.e.,

$$\begin{cases} du - \nabla \cdot (\kappa(x)\nabla u) dt = f(u)dt + g(x, t)dW(t) & \text{in } D \times (0, T], \\ u(x, t) = 0 & \text{on } \partial D \times (0, T], \\ u(x, 0) = u_0(x) & \text{in } D. \end{cases} \tag{3.17}$$

We similarly have the variational form of (3.17)

$$\begin{cases} (u_t, v) + a(u, v) = (f(u), v) + (g(x, t)\xi(t), v) & \forall v \in H_0^1, t > 0, \\ (u(\cdot, 0), v) = (u_0, v) & \forall v \in H_0^1, \end{cases} \quad (3.18)$$

Then CEM-GMsFEM solution  $u(\cdot, t) \in V_{ms}$  of (3.18) solves

$$\begin{cases} ((u_{ms})_t, v) + a(u_{ms}, v) = (f(u_{ms}), v) + (g(x, t)\xi(t), v) & \forall v \in V_{ms}, t > 0, \\ (u_{ms}(\cdot, 0), v) = (u_{0,ms}, v) & \forall v \in V_{ms} \end{cases} \quad (3.19)$$

We have the following error estimate of CEM-GMsFEM for the SPDE with additive noise, which generalizes the result in [42].

**THEOREM 3.4.** *Let  $u$  and  $u_{ms}$  be the solution of (3.18) and (3.19), respectively. Then for any fixed  $t \in [0, T]$ ,*

$$\begin{aligned} & \mathbf{E} \| (u - u_{ms})(t) \|_H^2 + \mathbf{E} \int_0^t \| u - u_{ms} \|_a^2 ds \\ & \leq Ch^2 \Lambda^{-1} \kappa_0^{-1} (\| f(u) \|_{\mathcal{H}}^2 + \mathbf{E} \| u_0 \|_a^2 + \mathbf{E} \| u_{0,ms} \|_a^2) + \mathbf{E} \| (u - u_{ms})(0) \|_H^2, \end{aligned} \quad (3.20)$$

where  $C$  is a constant independent of  $\kappa$  and the mesh size  $h$ .

*Proof.* From (3.18) and (3.19), for  $\forall v \in V_{ms}$ , we have

$$((u - u_{ms})_t, v) + a(u - u_{ms}, v) = (f(u) - f(u_{ms}), v). \quad (3.21)$$

The noise term disappears because diffusion  $g(x, t)$  is independent of the state  $u$ . By following the proof of Theorem 3.3, the proof is done.  $\square$

**4. Model reduction for nonlinear terms.** Let  $\{\varphi_i(x)\}_{i=1}^{N_r}$  be the set of multiscale basis functions in CEM-GMsFEM. Then we have an approximation,

$$u \approx u_{ms} = \sum_{i=1}^{N_r} u_{ms}^i(t) \varphi_i(x).$$

After we apply CEM-GMsFEM to SPDE(2.1), CEM-GMsFEM yields a discrete dynamical system of nonlinear ODE:

$$\begin{cases} \mathbf{M} \frac{d\mathbf{u}_{ms}}{dt} + \mathbf{A} \mathbf{u}_{ms}(t) = \mathbf{F}(\mathbf{u}_{ms}(t)) \\ \mathbf{u}_{ms}^0 = \mathbf{u}_{ms}(0), \end{cases} \quad (4.1)$$

where  $\mathbf{u}_{ms} = [u_{ms}^1, u_{ms}^2, \dots, u_{ms}^{N_r}]^T \in \mathbb{R}^{N_r}$  and

$$\begin{aligned} \mathbf{M}_{ij} &= \int_D \varphi_i(x) \varphi_j(x), \\ \mathbf{A}_{ij} &= \int_D \kappa(x) \nabla \varphi_i(x) \nabla \varphi_j(x), \\ \mathbf{F}(\mathbf{u}_{ms}(t))_i &\approx \int_D \left( f \left( \sum_{l=1}^{N_r} u_{ms}^l \varphi_l(x) \right) + g \left( \sum_{l=1}^{N_r} u_{ms}^l \varphi_l(x) \right) \xi(t) \right) \varphi_i(x). \end{aligned}$$

Notice that  $\mathbf{M}, \mathbf{A} \in \mathbb{R}^{N_r \times N_r}$ , and  $\mathbf{F} : \mathbb{R}^{N_r} \rightarrow \mathbb{R}^{N_r}$  is a nonlinear function. Although  $N_r$ , number of multiscale basis functions, is usually much smaller than number of fine-grid FEM basis functions, computation of the above system (4.1) is still challenging

because the high-dimensionality is still in the nonlinear term and we need to compute many trajectories for statistical estimation of the solution. Thus it is desirable to significantly reduce the nonlinear dynamic system.

In this section, we first briefly review two important model reduction methods: POD and DEIM. Finally we introduce a stochastic online DEIM, which can substantially improve the computation efficiency of the nonlinear stochastic system (4.1). For simplicity of presentation, we rewrite the system (4.1) by

$$\frac{d\mathbf{y}}{dt} = A\mathbf{y}(t) + \mathbf{f}(\mathbf{y}(t)). \quad (4.2)$$

Here we have abused the notation for linear coefficient matrix  $A$  and nonlinear function  $\mathbf{f}$  corresponding to  $\mathbf{M}^{-1}A$  and  $\mathbf{M}^{-1}\mathbf{F}$  respectively in (4.1), and  $\mathbf{y}$  represent the unknown solution that we are interested in.

**4.1. Proper orthogonal decomposition.** In the POD approach, we simulate the system by a reduced basis. Let  $\{\mathbf{y}(t_i)\}_{i=1}^M$  be the solution vectors at  $M$  time levels, and

$$Y = [\mathbf{y}(t_1), \mathbf{y}(t_2), \dots, \mathbf{y}(t_M)] \in \mathbb{R}^{n \times M}$$

be the snapshot matrix. POD constructs an orthogonal basis  $V \in \mathbb{R}^{n \times r}$ , in which the basis vectors are the first  $r \leq \text{rank}(Y)$  left singular vectors of  $Y$  corresponding to the first  $r$  largest singular values. The basis is also a solution of the following minimization problem

$$\min_{V \in \mathbb{R}^{n \times r}, V^T V = I_r} \|(I_n - VV^T)Y\|_F^2.$$

Thus POD-Galerkin method gives a reduced system of (4.2)

$$\frac{d\hat{\mathbf{y}}}{dt} = V^T A V \hat{\mathbf{y}}(t) + V^T \mathbf{f}(V \hat{\mathbf{y}}(t)), \quad (4.3)$$

and the solution  $\mathbf{y}(t)$  of (4.2) is approximated by  $\mathbf{y}(t) \approx V \hat{\mathbf{y}}(t)$ . However, solving the reduced system (4.3) instead of (4.2), we still need evaluations of the nonlinear term  $\mathbf{f}$  at all  $n$  components, the simulation of (4.3) is as expensive as solving the original system. DEIM can be used to overcome this difficulty.

**4.2. Discrete empirical interpolation method.** DEIM provides an approximation of the nonlinear function  $\mathbf{f}$  by a projection (interpolation), which maps a high  $n$ -dim space to a low  $m$ -dim space ( $m \ll n$ ) spanned by the basis  $\mathbf{U} = [\mathbf{u}_1, \mathbf{u}_2, \dots, \mathbf{u}_m] \in \mathbb{R}^{n \times m}$ . DEIM gives

$$\mathbf{f} \approx \mathbf{U}\mathbf{c}, \quad (4.4)$$

where  $\mathbf{c}$  is an unknown vector. The projection basis  $\mathbf{U}$  is obtained by applying POD to an appropriate set of the nonlinear snapshots

$$\{\mathbf{f}(\mathbf{y}(t_1)), \dots, \mathbf{f}(\mathbf{y}(t_M))\} \subset \mathbb{R}^n.$$

The system (4.4) is overdetermined. In order to solve it, we multiplies the equation by the transpose of the matrix  $P \in \mathbb{R}^{n \times m}$ ,

$$P^T \mathbf{f} = P^T \mathbf{U}\mathbf{c}.$$

Thus, if  $P^T \mathbf{U}$  is non-singular, then we can determine  $\mathbf{c} = (P^T \mathbf{U})^{-1} P^T \mathbf{f}$ . Therefore, we have an approximation of nonlinear term,

$$\mathbf{f} \approx \mathbf{U}(P^T \mathbf{U})^{-1} P^T \mathbf{f}. \quad (4.5)$$

In particular, DEIM chooses  $m$  pairwise different interpolation points  $p_1, \dots, p_m \in \{1, \dots, n\}$  and  $P = [e_{p_1}, e_{p_2}, \dots, e_{p_m}]$ , where  $e_{p_i} = [0, \dots, 0, \dots, 1, 0, \dots, 0]^T \in \mathbb{R}^n$  is the  $p_i$ -th unit vector. The interpolation points are chosen by a greedy method [12], which is specified by the basis matrix. The interpolation points matrix  $P$  and the DEIM basis  $\mathbf{U}$  are selected such that  $P^T \mathbf{U}$  has full rank. The approximation (4.5) implies that the nonlinear term  $\mathbf{f}$  can be only evaluated at  $m$  entries specified by  $P^T$  instead of all  $n$  components. Thus DEIM gives a reduced system,

$$\frac{d\hat{\mathbf{y}}}{dt} = V^T A V \hat{\mathbf{y}}(t) + V^T \mathbf{U}(P^T \mathbf{U})^{-1} P^T \mathbf{f}(V \hat{\mathbf{y}}(t)).$$

**4.3. Stochastic online DEIM.** For stochastic systems, we may have the nonlinear snapshots along several different trajectories  $\{\mathbf{y}^1, \mathbf{y}^2, \mathbf{y}^3, \dots, \mathbf{y}^k\}$  at times  $\{t_1, t_2, \dots, t_M\}$ :

$$\begin{aligned} \{\mathbf{f}(\mathbf{y}^1(t_1)), \dots, \mathbf{f}(\mathbf{y}^1(t_M))\} &\subset \mathbb{R}^n, \\ \{\mathbf{f}(\mathbf{y}^2(t_1)), \dots, \mathbf{f}(\mathbf{y}^2(t_M))\} &\subset \mathbb{R}^n, \\ \{\mathbf{f}(\mathbf{y}^3(t_1)), \dots, \mathbf{f}(\mathbf{y}^3(t_M))\} &\subset \mathbb{R}^n, \\ &\vdots \\ \{\mathbf{f}(\mathbf{y}^k(t_1)), \dots, \mathbf{f}(\mathbf{y}^k(t_M))\} &\subset \mathbb{R}^n. \end{aligned}$$

Although we can apply DEIM to each trajectory, the computation complexity will be proportional to the number of trajectories. To take account of this issue, we apply DEIM to mean of a few trajectories available. Let the mean snapshots

$$\{\mathbf{f}(\bar{\mathbf{y}}(t_1)), \dots, \mathbf{f}(\bar{\mathbf{y}}(t_M))\} \subset \mathbb{R}^n,$$

where  $\mathbf{f}(\bar{\mathbf{y}}(t_i)) = \mathbf{f}(\frac{1}{k} \sum_{j=1}^k \mathbf{y}^j(t_i))$   $i = 1, 2, \dots, M$ . Thus we get the approximation

$$\mathbf{f}(\bar{\mathbf{y}}(t)) \approx \bar{\mathbf{U}}(\bar{P}^T \bar{\mathbf{U}})^{-1} \bar{P}^T \mathbf{f}(\bar{\mathbf{y}}(t)),$$

where the DEIM basis  $\bar{\mathbf{U}}$  is obtained by the SVD of snapshot matrix  $[\mathbf{f}(\bar{\mathbf{y}}(t_1)), \dots, \mathbf{f}(\bar{\mathbf{y}}(t_M))]$ , and  $\bar{P}$  is the interpolation point matrix.

However, when a new trajectory is realised, i.e.,  $\{\mathbf{f}(\tilde{\mathbf{y}}(t_1)), \dots, \mathbf{f}(\tilde{\mathbf{y}}(t_M))\} \subset \mathbb{R}^n$  is available, the reduced model obtained by dealing with the mean of all previous trajectories may not capture the new information from the new trajectory. In order to take the new information, we introduce a stochastic online adaptive DEIM, which updates the orthogonal basis matrix online with respect to any new trajectory.

Based on the reduced model  $(\bar{\mathbf{U}}, \bar{P})$  obtained already in the offline phase, we provide the online updated basis  $\tilde{\mathbf{U}}$  to approximate the nonlinear function along any new trajectory, and repeatedly use the unchanged interpolation matrix  $\tilde{P} = \bar{P} \triangleq P$ . To this end, we need to evaluate the DEIM approximation quality of nonlinear function by a residual, and use the residual to construct a online adaptive basis.

The traditional DEIM interpolates  $\mathbf{f}(\bar{\mathbf{y}}(t))$  at the interpolation indexes, and we have a zero-valued residual

$$\mathbf{r}(\bar{\mathbf{y}}(t)) = \bar{\mathbf{U}}(P^T \bar{\mathbf{U}})^{-1} P^T \mathbf{f}(\bar{\mathbf{y}}(t)) - \mathbf{f}(\bar{\mathbf{y}}(t))$$

at the interpolation points. However, for a new trajectory, the residual

$$\mathbf{r}(\tilde{\mathbf{y}}(t)) = \bar{\mathbf{U}}(P^T \bar{\mathbf{U}})^{-1} P^T \mathbf{f}(\tilde{\mathbf{y}}(t)) - \mathbf{f}(\tilde{\mathbf{y}}(t))$$

is not zero any more, i.e.,

$$\|P^T \mathbf{r}(\tilde{\mathbf{y}}(t))\|_2 > 0.$$

As in section 4.2, we have

$$\mathbf{c}(\tilde{\mathbf{y}}(t)) = (P^T \bar{\mathbf{U}})^{-1} P^T \mathbf{f}(\tilde{\mathbf{y}}(t)),$$

and  $\mathbf{C} \in \mathbb{R}^{m \times M}$  is the coefficient matrix with the coefficients  $\mathbf{c}(\tilde{\mathbf{y}}(t_1)), \mathbf{c}(\tilde{\mathbf{y}}(t_2)), \dots, \mathbf{c}(\tilde{\mathbf{y}}(t_M))$  as columns. Then we update the basis  $\tilde{\mathbf{U}} = \bar{\mathbf{U}} + \Delta \mathbf{U}$  such that the updated basis minimizes Frobenius norm of the residual at the observation time levels, i.e.,

$$\tilde{\mathbf{U}} = \arg \min_{\mathbf{U}} \|P^T (\mathbf{U}\mathbf{C} - \mathbf{F})\|_F^2, \quad (4.6)$$

where  $\mathbf{F} = [\mathbf{f}(\tilde{\mathbf{y}}(t_1)), \dots, \mathbf{f}(\tilde{\mathbf{y}}(t_M))] \in \mathbb{R}^{n \times M}$  is the evaluation of the nonlinear function along the new trajectory. Similar to Section 4.2, only  $P^T \mathbf{F} \in \mathbb{R}^{m \times M}$  is required in (4.6), not the complete matrix  $\mathbf{F} \in \mathbb{R}^{n \times M}$ . Let the approximation residual matrix  $\mathbf{R} = \bar{\mathbf{U}}\mathbf{C} - \mathbf{F}$ . Then we solve the minimization problem

$$\arg \min_{\Delta \mathbf{U} \in \mathbb{R}^{n \times m}} \|P^T \mathbf{R} + P^T \Delta \mathbf{U}\mathbf{C}\|_F^2. \quad (4.7)$$

We note that the unknown matrix  $\Delta \mathbf{U}$  is both premultiplied and postmultiplied. The optimization problem (4.7) is technically tricky. To overcome the difficulty, we decompose it into two optimization problems, and use the Moore-Penrose pseudo-inverse to solve it approximately,

$$\arg \min_{\mathbf{b} \in \mathbb{R}^{n \times M}} \|P^T \mathbf{b} + P^T \mathbf{R}\|_F^2, \quad (4.8)$$

$$\arg \min_{\Delta \mathbf{U} \in \mathbb{R}^{n \times m}} \|\Delta \mathbf{U}\mathbf{C} - \mathbf{b}\|_F^2. \quad (4.9)$$

Since the interpolation matrix is a permutation matrix, which is invertible, we have  $\mathbf{b} = -\mathbf{R}$  from (4.8). After taking a transposition in (4.9), we have

$$\Delta \mathbf{U} = \mathbf{b} ((\mathbf{C}^T)^\dagger)^T = -\mathbf{R}\mathbf{C}^T (\mathbf{C}\mathbf{C}^T)^{-1}.$$

This is an approximation of (4.7).

Finally, We end this section with Algorithm 1, where we give the main steps of the stochastic online DEIM.

**Algorithm 1** Stochastic Online DEIM**Input:** nonlinear snapshots along multiple realizations

$$\{\mathbf{f}(\mathbf{y}^i(t_1)), \dots, \mathbf{f}(\mathbf{y}^i(t_M))\}_{i=1}^k \subset \mathbb{R}^n$$

**Output:** Online updated basis matrix  $\tilde{\mathbf{U}}$ , interpolation matrix  $P$ , reduced approximation  $\mathbf{f}$ **1:** Get mean snapshots matrix  $[\mathbf{f}(\bar{\mathbf{y}}(t_1)), \dots, \mathbf{f}(\bar{\mathbf{y}}(t_M))]$ ,where  $\mathbf{f}(\bar{\mathbf{y}}(t_i)) = \mathbf{f}(\frac{1}{k} \sum_{j=1}^k \mathbf{y}^j(t_i))$ ,  $i = 1, \dots, M$ **2:** Apply DEIM to mean snapshots matrix, and get  $(\bar{\mathbf{U}}, \bar{P})$ **3:** Compute coefficient matrix  $\mathbf{C}$ , with columns  $\{\mathbf{c}(\tilde{\mathbf{y}}(t_i)) = (\bar{P}^T \bar{\mathbf{U}})^{-1} \bar{P}^T \mathbf{f}(\tilde{\mathbf{y}}(t_i))\}_{i=1}^M$ **4:** Compute residual matrix  $\mathbf{R} = \bar{\mathbf{U}}\mathbf{C} - \mathbf{F}$ , where  $\mathbf{F} = [\mathbf{f}(\tilde{\mathbf{y}}(t_1)), \dots, \mathbf{f}(\tilde{\mathbf{y}}(t_M))]$ **5:** Solve optimization problem and have  $\Delta \mathbf{U} = -\mathbf{R} ((\mathbf{C}^T)^\dagger)^T$ **6:** Update basis matrix  $\tilde{\mathbf{U}} = \bar{\mathbf{U}} + \Delta \mathbf{U}$ , and remain interpolation matrix  $P = \bar{P}$  unchanged**7:** Approximate  $\mathbf{f}(\tilde{\mathbf{y}}(t)) \approx \tilde{\mathbf{U}}(P^T \tilde{\mathbf{U}})^{-1} P^T \mathbf{f}(\tilde{\mathbf{y}}(t))$ 

**5. Numerical results.** In this section, we present several numerical examples to verify the previous analysis and demonstrate the efficacy of stochastic online model reduction approach. In the numerical simulations of this paper, we will not focus on the coarsening effect in CEM-GMsFEM because there exist many literatures [10, 29] that have extensively addressed it. In Section 5.1, we compare the behaviours of CEM-GMsFEM in deterministic system and stochastic system. In Section 5.2, some different methods are applied to an SPDE and show the advantage of Online DEIM over other variants of DEIM. A coupled stochastic porous media dynamical system is considered in Section 5.3 to illustrate the applicability of Online DEIM-MS in coupled systems.

For the numerical examples in this section, the computational spatial domain is  $D = [0, 1] \times [0, 1]$ . We divide the domain  $D$  into a  $100 \times 100$  fine grid, and the coarse grid is  $10 \times 10$ . We take number of local basis functions  $L_i = 4$  and oversampling layers  $m = 4$  by the empirical numerical results in [29]. We will keep the same setting for  $L_i, m$  in the simulations. The solution with FEM on the fine grid is used as the reference solution. For simplicity of presentation, we will use MS solution to denote CEM-GMsFEM solution in figures and tables.

**5.1. Comparison in a deterministic system and a stochastic system.**

Firstly, we will illustrate the difference of the behaviours of CEM-GMsFEM between a deterministic system and a stochastic system. They are specified as following,

$$(d) \begin{cases} \frac{\partial u}{\partial t} - \nabla \cdot (\kappa(x) \nabla u) = 10 \cos(u) & \text{in } D \times (0, T], \\ u(x, t) = 0 & \text{on } \partial D \times (0, T], \\ u(x, 0) = 2\pi \sin(2\pi x_1) \sin(2\pi x_2) & \text{in } D, \end{cases} \quad (5.1)$$

$$(s) \begin{cases} du - \nabla \cdot (\kappa(x) \nabla u) dt = 10 \cos(u) dt + (u^2 + 10) dW(t) & \text{in } D \times (0, T], \\ u(x, t) = 0 & \text{on } \partial D \times (0, T], \\ u(x, 0) = 2\pi \sin(2\pi x_1) \sin(2\pi x_2) & \text{in } D. \end{cases} \quad (5.2)$$

The multiscale coefficient  $\kappa(x)$  in the above equations is depicted in Figure 5.1.

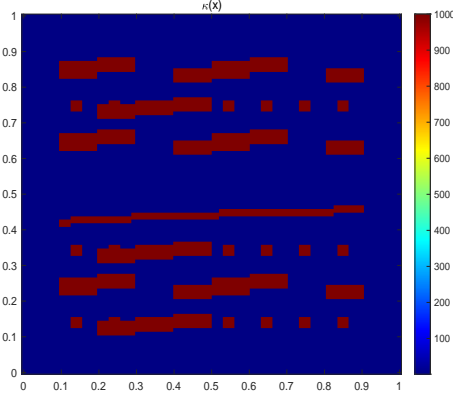
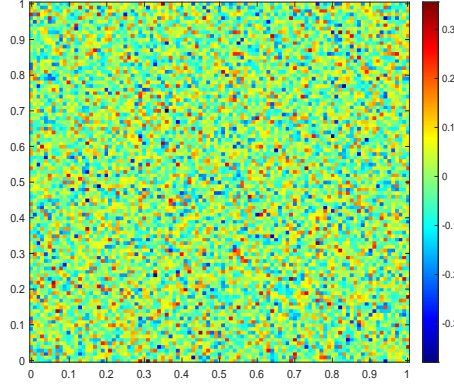
FIG. 5.1. Multiscale coefficient  $\kappa(x)$ 

FIG. 5.2. Brownian motion increment

For the stability of numerical method, we choose the stochastic full-implicit scheme to treat the temporal discretization. Then the full discretization reads as

$$u_{m_s}^{k+1} = u_{m_s}^k + A_\kappa u_{m_s}^{k+1} \Delta t_k + f(u_{m_s}^{k+1}) \Delta t_k + g(u_{m_s}^k) \Delta W_k.$$

The temporal is partitioned uniformly by the interval  $\Delta t = 0.01$ . We consider the Brownian motion with three different covariance coefficients  $Q = 0.01, 1, 100$  as three degenerated  $Q$ -Wiener processes. Figure 5.2 shows a sample of Brownian motion increment with time interval  $\Delta t$  and covariance coefficients  $Q = 1$ . Since the drift term  $\cos(u)$  is nonlinear, we get a nonlinear equation of the unknown state  $u_{m_s}^{k+1}$ , and use Newton iteration to solve the nonlinear system. Because we focus on the performance of CEM-GMsFEM, we do not use any DEIM to reduce the nonlinear model in this subsection. We will compute the CEM-GMsFEM solutions of the deterministic and stochastic systems with the three different coefficients  $Q$ .

Figure 5.3 shows solutions of deterministic system and stochastic system at  $t = 1$ . For the stochastic system, mean of solutions is approximated by averaging 100 stochastic realizations. We notice that individual behaviour (middle) and mean behaviour (right) are almost same because of a small coefficient  $Q$  in the stochastic system. Their solution profiles are almost the same as the solution of deterministic system.

To evaluate the approximation accuracy, Figure 5.4 shows the relative  $L_2$  error and relative energy error of CEM-GMsFEM solutions. Here we take the 100 stochastic realizations to approximate expectation of stochastic solutions and reference solution is the FEM solution in fine grid. From this figure, we see that error of the individual trajectory of CEM-GMsFEM solution is much larger than the other two errors:  $MS_d$  and mean of  $MS_s$ . This shows that randomness of individual path may impact on the approximation of CEM-GMsFEM because we do not consider stochastic term when we construct the basis functions of CEM-GMsFEM. Moreover,  $L_2$  error of mean of  $MS_s$  is almost the same as the error of  $MS_d$ , while energy error of mean of  $MS_s$  is slightly larger than  $MS_d$ .

When the covariance coefficient  $Q$  of Wiener-process increases, the trajectories of SPDE may show significant difference among them. By the middle plot in Figure 5.5 ( $Q = 1$ ), the first trajectory of the SPDE solution shows a random perturbation comparing to deterministic model solution and mean of SPDE solution. However,



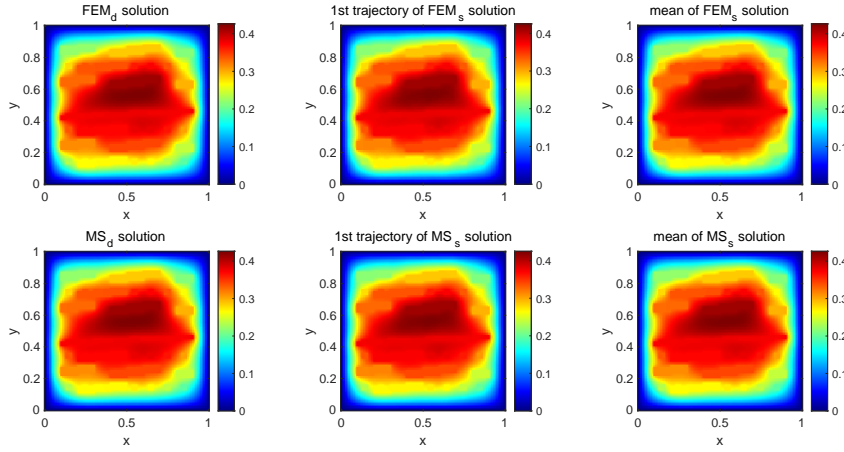


FIG. 5.3. Solution profiles at  $t = 1$ . Top left: FEM reference solution of deterministic system; Top middle: the first trajectory of FEM reference solution of stochastic system with covariance coefficient  $Q = 0.01$ ; Top right: the mean of FEM reference solution of stochastic system; Bottom: Corresponding CEM-GMsFEM solutions.

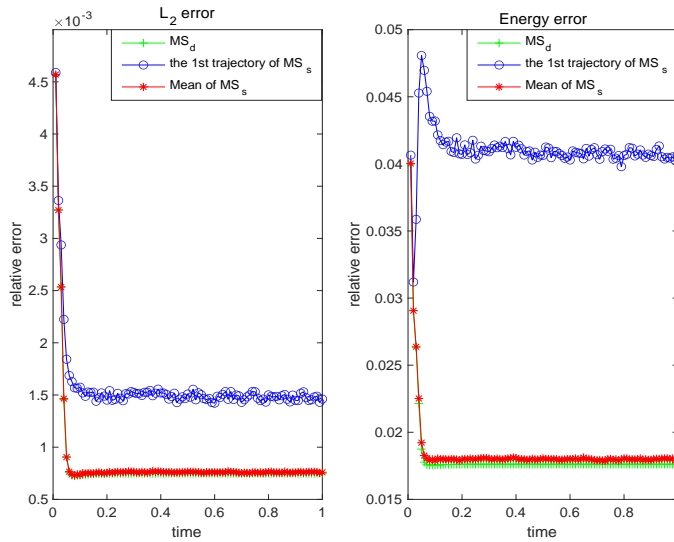


FIG. 5.4. Relative  $L_2$  errors (left) and relative energy errors (right) for MS solution (green +) of deterministic problem, MS solution mean (red \*) and one trajectory of MS solution (blue o),  $Q = 0.01$ .

mean of stochastic FEM solution behaves more like FEM<sub>d</sub> solution. Figure 5.5 ( $Q = 1$ ) shows that CEM-GMsFEM solutions approximate the FEM solutions in fine grid. As  $Q = 0.01$  case, we illustrate  $L_2$  relative error and energy relative error of CEM-GMsFEM solutions in Figure 5.6 with FEM solutions as reference solutions. We see that, for the stochastic model,  $L_2$  error and energy error of the first path are both much larger than deterministic CEM-GMsFEM solution. The error of mean of CEM-

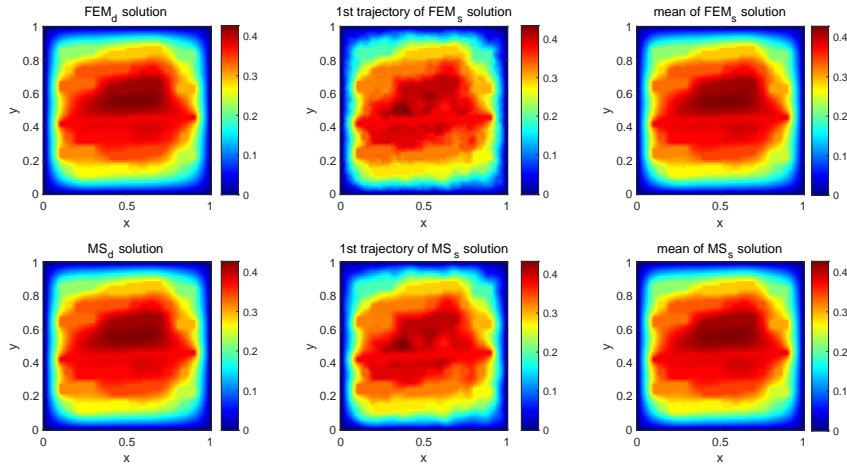


FIG. 5.5. Solution profiles at  $t = 1$ . Top left: FEM reference solution of deterministic system; Top middle: the first trajectory of FEM reference solution of stochastic system with covariance coefficient  $Q = 1$ ; Top right: the mean of FEM reference solution of stochastic system; Bottom: Corresponding CEM-GMsFEM solutions.

GMsFEM solution to the stochastic model is also slightly larger than the error of CEM-GMsFEM solution to the deterministic model. The reason may be from Monte Carlo sampling.

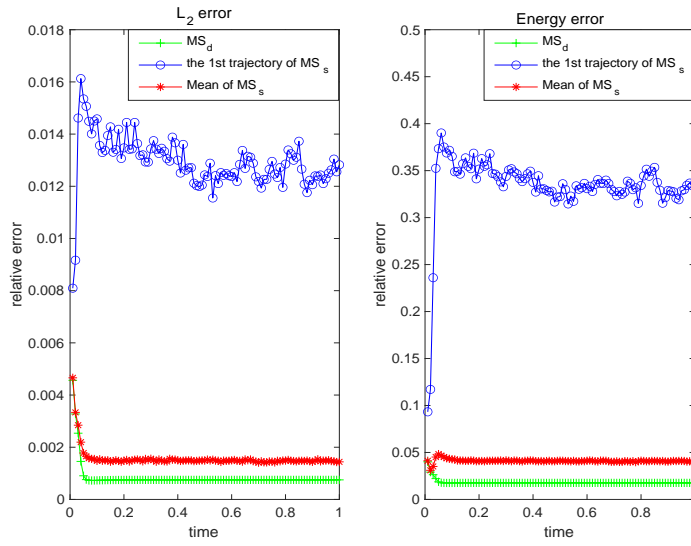


FIG. 5.6. Relative  $L_2$  errors (left) and relative energy errors (right) for MS solution (green +) of deterministic problem, MS solution mean (red \*) and one trajectory of MS solution (blue o).  $Q = 1$ .

Comparing Figure 5.7 ( $Q = 100$ ) with Figure 5.3 and Figure 5.5, we observe that the larger of the covariance coefficient  $Q$  leads to less accuracy of CEM-GMsFEM.

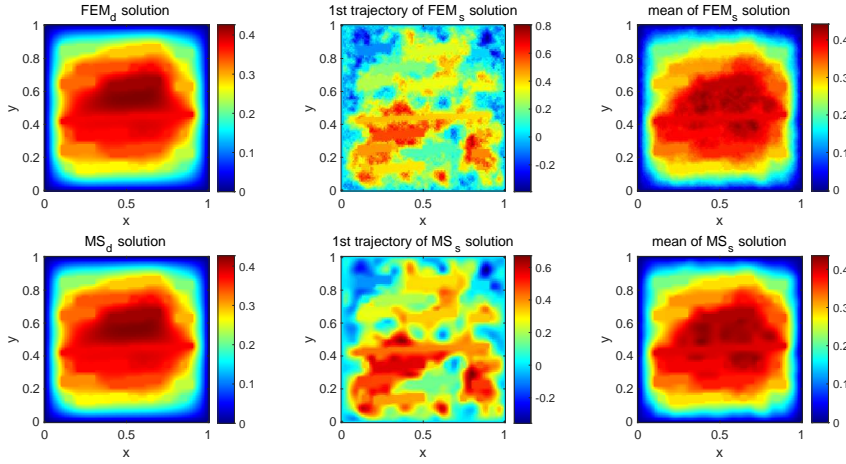


FIG. 5.7. Solution profiles at  $t = 1$ . Top left: FEM reference solution of deterministic system; Top middle: the first trajectory of FEM reference solution of stochastic system with covariance coefficient  $Q = 100$ ; Top right: the mean of FEM reference solution of stochastic system; Bottom: Corresponding CEM-GMsFEM solutions.

This is because we construct the multiscale basis functions without considering the stochastic influence, i.e., the stochastic perturbation of the Wiener process. By Figure 5.8, we also see that the error of mean of CEM-GMsFEM solution is much smaller than the error of individual trajectory.

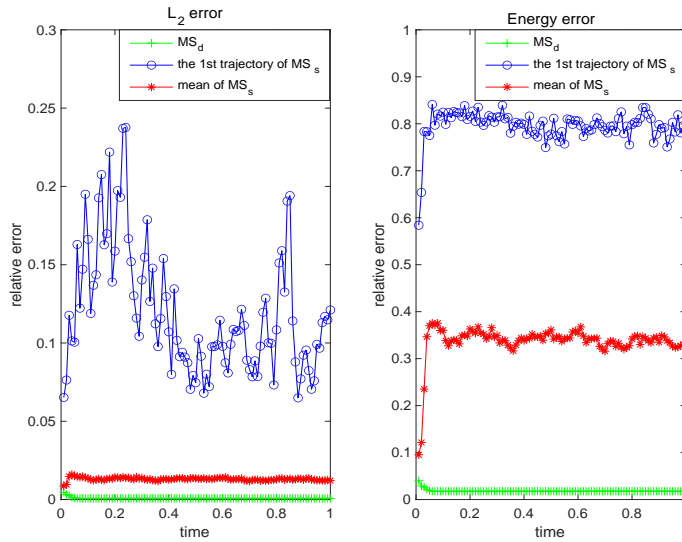


FIG. 5.8.  $L_2$  Relative  $L_2$  errors (left) and relative energy errors (right) for MS solution (green +) of deterministic problem, MS solution mean (red \*) and one realization of MS solution (blue o).  $Q = 100$ .

Moreover, we compare the CPU time of the different methods. For the nonlinear

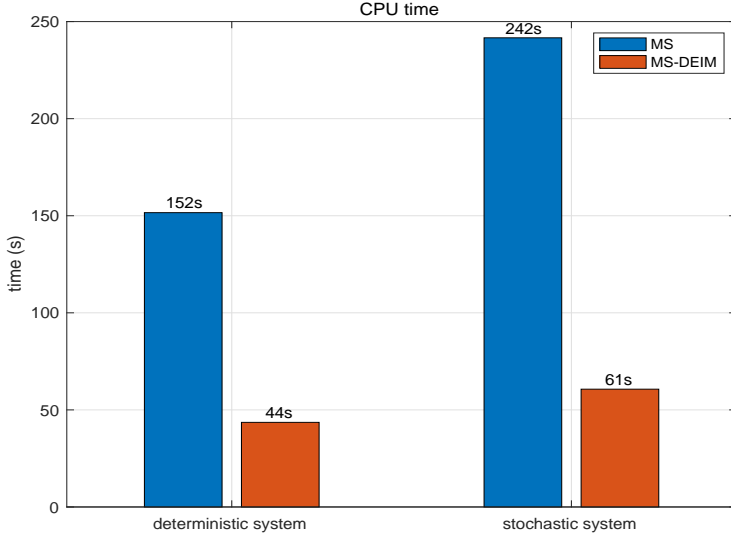


FIG. 5.9. CPU time for the deterministic model and the stochastic model.

terms, we use two different models for simulation: full-order model and DEIM reduced model. Figure 5.9 illustrates the CPU time for deterministic model and stochastic model using two different methods: CEM-GMsFEM (MS) and CEM-GMsFEM-DEIM (MS-DEIM). By the figure, we find that the CPU time for stochastic model is longer than the deterministic model. This is because that extra computation is required for the diffusion term of white noise. The figure also clearly shows that DEIM take much less time than Newton method for both deterministic nonlinear model and stochastic nonlinear model.

**5.2. Stochastic online DEIM with CEM-GMsFEM.** In this subsection, we will focus on the stochastic online DEIM incorporating with CEM-GMsFE method. The approach is referred to as Online DEIM-MS for abbreviation. We concentrate on two important problems about the approach: effect of snapshots in DEIM and performance of individual stochastic realization.

**5.2.1. Effect of snapshot in offline phase and online phase of DEIM.** Stochastic online DEIM needs to use snapshots from offline phase and online phase: the offline snapshots consist of mean information, and online snapshots consist of new trajectory information. Thus different choices of snapshots in offline and online phase produce the different variants of online DEIM.

In this subsection, we compute the relative errors from the online DEIM using different snapshots and explore the impact of the offline snapshots and online snapshots. Meanwhile, FEM solution and CEM-GMsFEM solution are also computed to assess the effectiveness of online DEIM-MS. For numerical simulation, we solve the following SPDE,

$$\begin{cases} du - \nabla \cdot (\kappa(x)\nabla u)dt = \cos(u)dt + (u^2 + 2)dW(x, t) & \text{in } D \times (0, T], \\ u(x, t) = 0 & \text{on } \partial D \times (0, T], \\ u(x, 0) = \sin(2\pi x_1) \sin(2\pi x_2) & \text{in } D, \end{cases} \quad (5.3)$$

where the temporal partition and multiscale coefficient  $\kappa(x)$  are chosen same as the example 5.1.

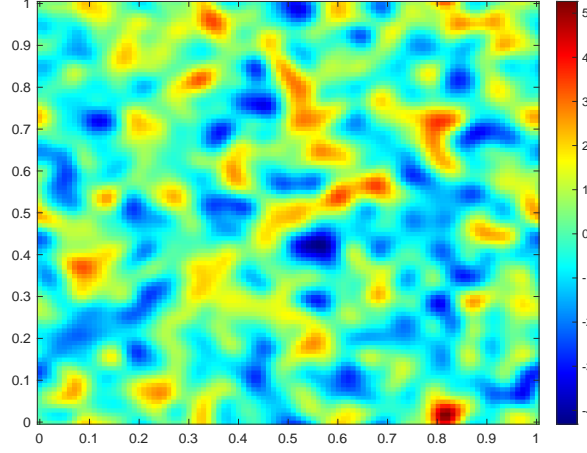


FIG. 5.10. A sample of the  $\mathcal{Q}$ -Wiener process increment  $\Delta W^J(x, t)$

In this subsection, we use a space-time  $\mathcal{Q}$ -Wiener process described in [30]. The covariance operator  $\mathcal{Q}$  has the eigenfunctions

$$e_{j_1, j_2}(x) = \frac{1}{\sqrt{a_1 a_2}} e^{2\pi i j_1 x_1 / a_1} e^{2\pi i j_2 x_2 / a_2}$$

and eigenvalues  $\mu_{j_1, j_2} = e^{-\alpha \gamma_{j_1, j_2}}$ ,  $\alpha > 0$  and  $\gamma_{j_1, j_2} = j_1^2 + j_2^2$ . The approximation of  $W(x, t)$  can be defined by

$$W^J(x, t) := \sum_{j_1 = -J_1/2+1}^{J_1/2} \sum_{j_2 = -J_2/2+1}^{J_2/2} \sqrt{\mu_{j_1, j_2}} e_{j_1, j_2}(x) \beta_{j_1, j_2}(t). \quad (5.4)$$

We illustrate a sample of  $\mathcal{Q}$ -Wiener process increment with  $J_1 = J_2 = 100$ ,  $\alpha = 0.0005$  in Figure 5.10.

For offline snapshots in DEIM, we compute 100 solutions of trajectories to get mean information. Here, we compare three different cases of offline-online. In Case I, we take mean of nonlinear evaluation in the first half time interval, i.e.,

$$f(\bar{u}(x, t)), g(\bar{u}(x, t)), (x, t) \in D \times [0, T/2],$$

as the mean snapshots in the offline phase, and take the nonlinear evaluation of new realization in the first half interval as new data to update the stochastic online DEIM basis matrix in the online phase. In Case II, mean of evaluation of nonlinear functions in whole time interval, i.e.  $f(\bar{u}(x, t)), g(\bar{u}(x, t)), (x, t) \in D \times [0, T]$ , is used in the offline phase, and online phase is the same as Case I. In Case III, offline procedure is the same as Case I, but we use the nonlinear evaluation of new trajectory in the whole time interval to update online DEIM basis in online phase. And for case III, we keep the same number of snapshots as Case I in online phase by selecting snapshots sparsely.

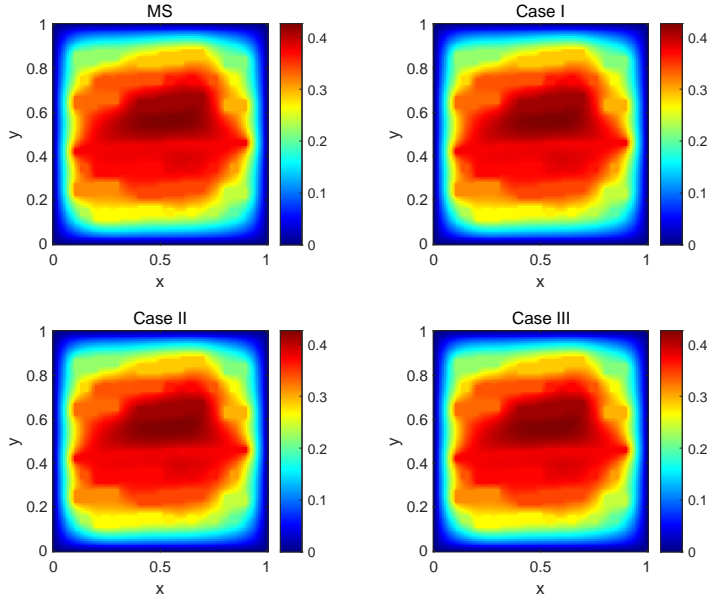


FIG. 5.11. Solution profiles at time  $t = 1$ . Left top: CEM-GMsFEM solution; Right top: Case I; Left bottom: Case II; Right bottom: Case III.

Thus, for Case I and Case II, solutions of a new sample in the first half temporal interval demonstrate good fitness of these two techniques, while models' prediction ability are showed by the accuracy of solution in the domain  $D \times (T/2, T]$ .

Figure 5.11 depicts CEM-GMsFEM solution and the Online DEIM-MS solutions associated to Case I, Case II and Case III. By the figure, the solution profiles look the same, and Online DEIM-MS is able to give a good approximation.

The  $L_2$  errors and energy errors of above methods are showed in Figure 5.12. From the figure, we see that the  $L_2$  errors are almost less than 0.1%, and the  $L_2$  error of Case I is the largest and the other two are smaller. This indicates that the use of longer time information as snapshots leads to more accurate solution. Besides, we find that CEM-GMsFEM using Newton method has the smallest error. This is consistent with our expectation. The figure shows that the errors tend to be stable as time increases. This may be because the system becomes stationary gradually.

**5.2.2. Individual performance.** In this numerical example, we are going to show the individual performance of online DEIM by presenting some new trajectories. We choose the same multiscale coefficient  $\kappa$  and  $\mathcal{Q}$ -Wiener process as example 5.1 with noise coefficient  $Q = 1, 100$ . In the example, we set the nonlinear functions  $f(u) = 2\pi \cos(u)$ ,  $g(u) = u^2 + 2$  and the initial condition  $u(x, 0) = 10 \sin(2\pi x_1) \sin(2\pi x_2)$ . We solve the SPDE using Online DEIM (Case I in Subsection 5.2.1) combining with CEM-GMsFEM. FEM solution in fine grid is the reference solution.

Figure 5.13 shows the solution profiles of three different stochastic realizations when covariance  $Q = 1$ . The profiles of different trajectories are similar because of small covariance coefficient  $Q$ . The figure clearly shows that the individual performance of Online DEIM-MS solution approximates well reference solution for each

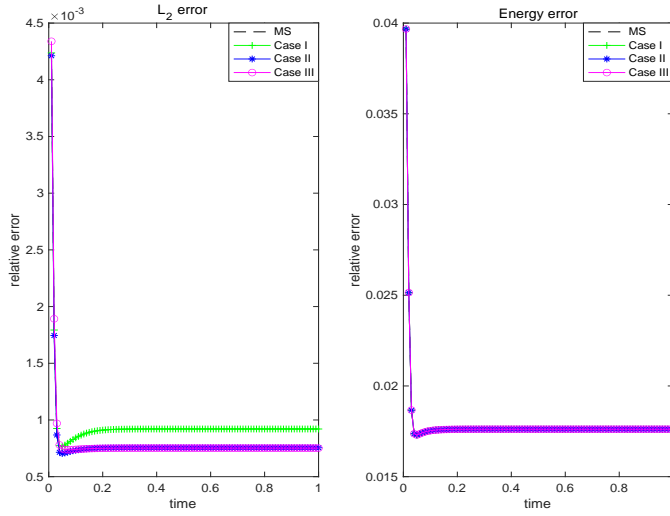


FIG. 5.12. Relative  $L_2$  errors (left) and relative energy errors (right) versus time  $t$ .

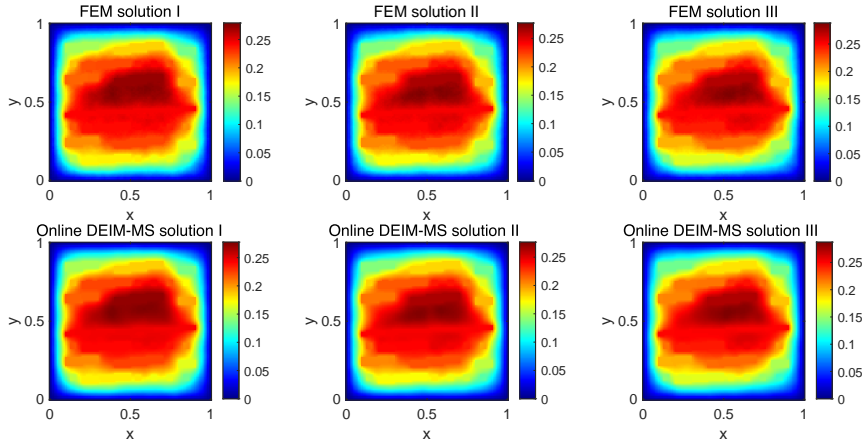


FIG. 5.13. Solution profiles for three arbitrary trajectories,  $Q = 1$ . Top: FEM reference solutions; Bottom: Online DEIM-MS solutions (I II III are the three different trajectories).

trajectory.

Figure 5.14 depicts the solution profiles when  $Q = 100$ . Because the diffusion covariance is large, individual profiles are quite different from the three different realizations. But the Online DEIM-MS solution looks very like the FEM solutions in general. That is to say, the individual trajectory performs accurately even though the diffusion covariance becomes large.

In Figure 5.15, we illustrate  $L_2$  errors, energy errors and deviations of the arbitrary three realizations. Here the deviations are given by

$$\text{deviation} = \sqrt{\frac{\|\text{FEM solution of arbitrary realization} - \text{mean of FEM solutions}\|_2}{\|\text{mean of FEM solutions}\|_2}}$$

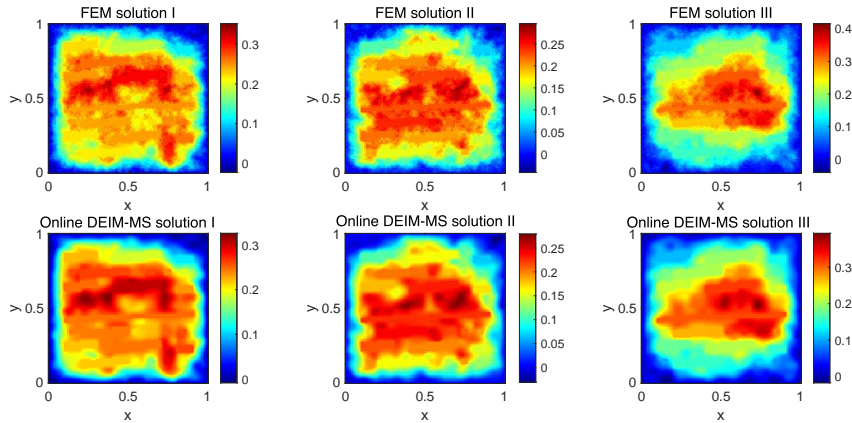


FIG. 5.14. Solution profiles for three arbitrary trajectories,  $Q = 100$ . Top: FEM reference solutions; Bottom: Online DEIM-MS solutions (I II III are three different trajectories).

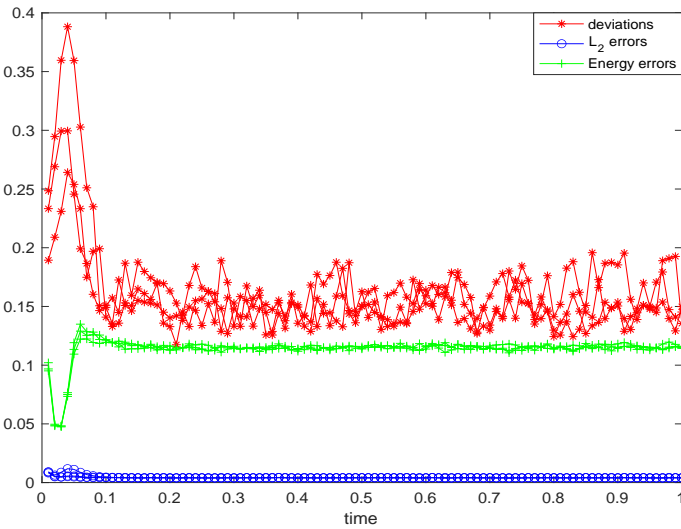


FIG. 5.15. Relative  $L_2$  errors (blue  $\circ$ ), relative energy errors (green  $+$ ) and deviations for the three arbitrary trajectories,  $Q = 100$ .

Large deviation means that the problem has a very different new realization from the mean information. It is obvious in Figure 5.15 that the deviations are much larger than the errors. Thus large deviations and small errors indicate the good performance of Online DEIM-MS for new trajectories. One can predict how the state evolves with respect to time.

In Table 5.1, we make a comparison of the approximation error and the computational cost between stochastic Online DEIM and traditional DEIM, referred as Offline DEIM when these methods are applied to a single trajectory. Since their offline phases are the same, we only record the time of online phases. For Offline DEIM, the CPU time is the time of CEM-GMsFEM computation with offline-reduced nonlinear func-



tions. But for Online DEIM, the CPU time includes both the time of online update of DEIM basis matrix and the time of MS computation with online-reduced nonlinear functions. And the relative  $L_2$  error and relative energy error are both listed in the table.

TABLE 5.1  
A comparison of CPU time and relative errors.

Method	CPU time(s)	$L_2$ error	Energy error
MS	209.7017	$5.5858 \times 10^{-3}$	$7.3928 \times 10^{-2}$
Offline DEIM-MS	53.4225	$7.3864 \times 10^{-3}$	$7.4025 \times 10^{-2}$
Online DEIM-MS	53.4835	$6.6042 \times 10^{-3}$	$7.3973 \times 10^{-2}$

Table 5.1 shows that Online DEIM has better accuracy while it takes slightly more time than Offline DEIM. Comparing with CEM-GMsFEM without any reduction, Online DEIM is able to significantly improve the computation efficiency and keep good accuracy.

**5.3. A coupled stochastic system in porous media.** In this subsection, we consider a coupled system, in which SDE is coupled to a porous media equation. In this class of system, the fluid velocity is affected by the particle deposition, and the effect is described by a stochastic differential equation where the particle velocity is influenced by the fluid velocity in turn. That is to say, the particle dynamics (i.e., the stochastic differential equation in (5.5)) governs the permeability change. Thus the coupled system produces a stochastic porous media problem in the real world. Here is a specific system:

$$\begin{cases} \frac{\partial u(x,t)}{\partial t} = \nabla \cdot (\kappa(x)\nabla u) + 10e^{2v} \sin(u) & \text{in } D \times (0, T], \\ dv(x,t) = -10(v-u)dt + \frac{1}{\sqrt{0.1}}dW(t) & \text{in } D \times (0, T], \\ u(x,t) = 0 & \text{on } \partial D \times (0, T], \\ u(x,0) = 1 & \text{in } D, \\ v(x,0) = 2 & \text{in } D, \end{cases} \quad (5.5)$$

where  $u$  represents the fluid velocity and  $v$  is the particle velocity. Here the permeability field  $\kappa(x)$  is taken as the Tenth Society of Petroleum Engineers Comparative Solution Project (SPE10), which is shown in Figure 5.16.

The model (5.5) describes an equation with the heterogeneous diffusion  $\kappa(x)$ , and  $e^{2v}$  characterizes the affection by particle deposition, and 10 times of fluid velocity affects the particle velocity. We choose constant 1 and 2 as initial velocity of fluid and of particle respectively, because the particle dynamics usually occurs faster compared to fluid flow. Besides, the long time evolution of system will cause the effect that solution  $u$  has the sharp decay to zero, and the solution becomes small after some time. To show the difference between different DEIM-MS approaches, we solve the problem in domain  $D = [0, 1] \times [0, 1]$ , with time interval  $t \in [0, 0.1]$ . In this example, we divide the time into  $N = 100$  intervals with step size  $\Delta t = 0.001$ , and compute 100 trajectories' solutions to get mean snapshots, and  $Q = 0.01$  for the Wiener process  $W(t)$ .

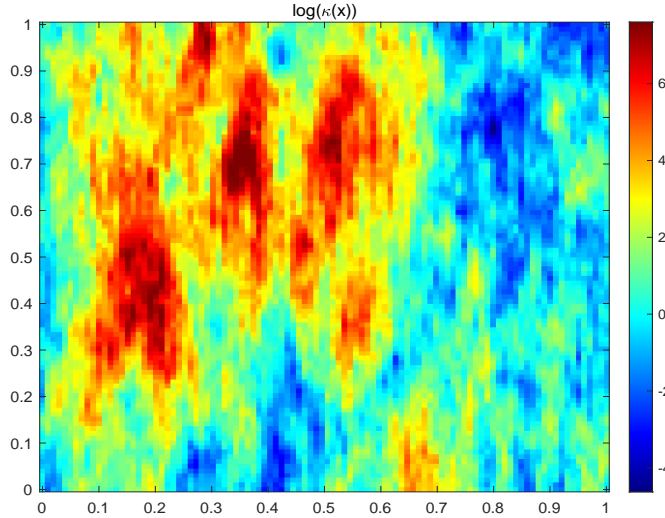


FIG. 5.16. A permeability field (a layer from SPE10)

We solve the coupled system sequentially (the semilinear PDE is solved after SDE), and we use drift-implicit Milstein scheme to solve SDE, while PDE is solved by four different methods : MS, Offline DEIM-MS, Online DEIM-MS and FEM in fine grid. We compute Offline DEIM-MS solution by the reduced model constructed in the offline phase where we utilize only the snapshots of nonlinear function  $e^{2v} \sin(u)$  along mean of offline trajectories, while Online DEIM-MS solution is computed by Case I in Section 5.2.

Figure 5.17 shows the profiles of fluid velocity  $u$ . By the figure, Online DEIM-MS solution at time  $t = 0.055$  is more close to the MS and FEM solution, while Offline DEIM-MS solution obviously differs from reference solution in some locations. This shows that Online DEIM-MS is better than Offline DEIM-MS for prediction.

Figure 5.18 shows the relative errors versus time. By the figure, we observe that the error of MS solution is the smallest. This coincides with the previous examples. In the offline phase, mean information in the first half time interval is used to construct the snapshots, compute the DEIM basis matrix and interpolation matrix. This yields a reduced model using Offline DEIM and Online DEIM. Moreover, for Online DEIM, we also utilize the data of new path to update the basis matrix in the online phase. Therefore, for  $t \in [0, T/2)$ , where  $T = 0.1$ , Online DEIM produces the fitness of system evolution, while for  $t \in (T/2, T]$ , Online DEIM can predict the propagation of system. But the prediction may perform well only in a short time interval, since the correlation will decay with the elapse of time. Comparing the error curve in Figure 5.18, we see that Online DEIM-MS is much more precise than Offline DEIM-MS for  $t \in [0, T/2)$ . For  $t \in (T/2, T]$ , the error of Online DEIM-MS increases over time as expected. Although the error of Online DEIM-MS grows in the later half interval, it is still much less than the error of Offline DEIM-MS. This implies that the prediction of Online DEIM is better than Offline DEIM. This verifies the accuracy of fitness and forecast of Online DEIM-MS approach.

In Figure 5.19, we give the profiles of particle velocity  $v$  at time  $t = 0.055$ . We

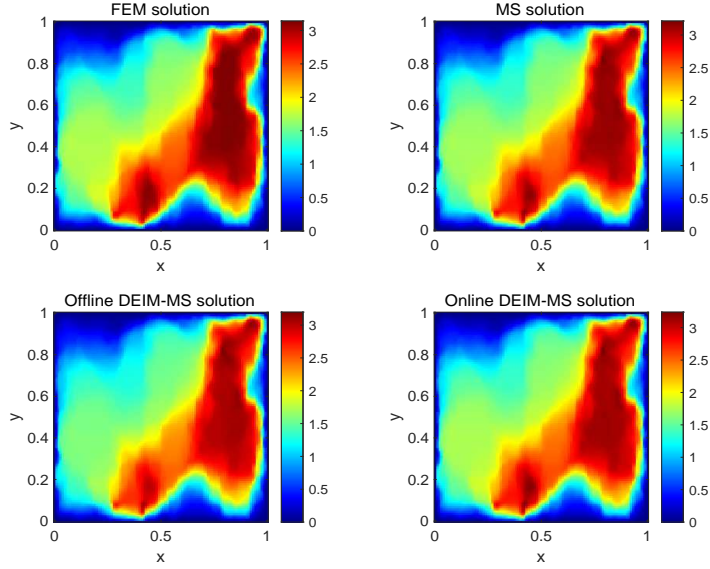


FIG. 5.17. Solution profiles of fluid velocity  $u$

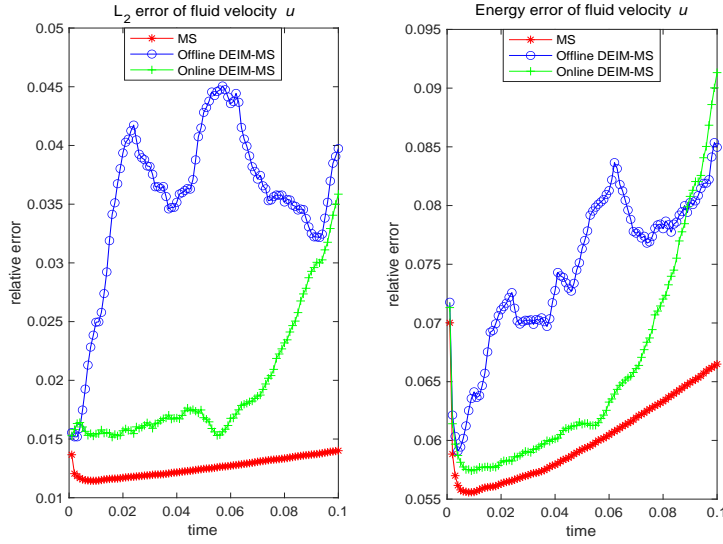


FIG. 5.18. Relative  $L_2$  errors (left) and energy errors (right) of fluid velocity  $u$  versus time  $t$

note that  $v$  is solved by plugging  $u$  into the stochastic equation. The solution  $u$  is computed by four different methods: FEM in fine grid, MS, Offline DEIM-MS and Online DEIM-MS. Different solutions of  $u$  lead to different solutions of  $v$  because they are coupled each other. By the figure, we find that the solution profiles are very close to each other. Comparing with Figure 5.17, the particle velocity  $v$  is not as smooth as the fluid velocity, due to the direct impact from Brownian motion. However, the

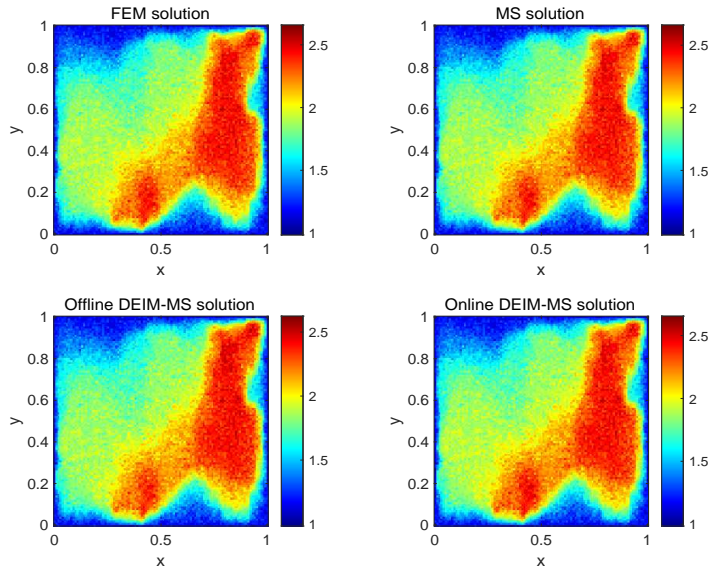


FIG. 5.19. Solution profiles of particle velocity  $v$  at  $t = 0.055$ .

particle and the fluid velocity have the similar pattern because the particle dynamics and the fluid dynamics interact on each other. We see that, for arbitrary  $t \in [0, T]$ , the error of Offline DEIM-MS solution is larger than that of Online DEIM-MS. The trend of error of particle velocity is consistent with the error of fluid velocity.

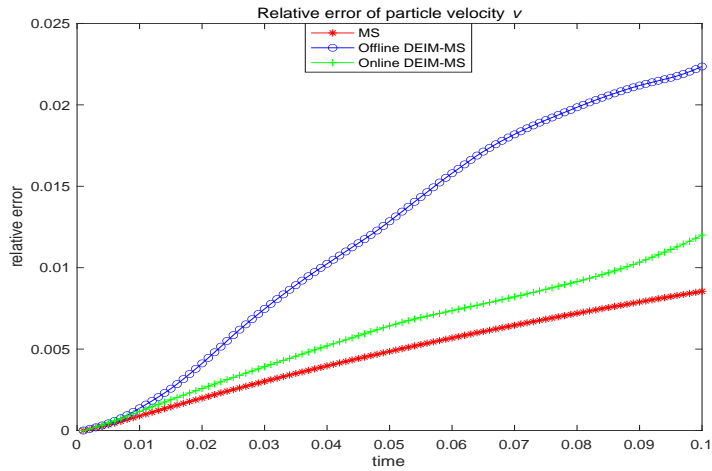


FIG. 5.20. Relative  $L_2$  errors of the particle velocity  $v$  versus time  $t$

**6. Conclusion.** We presented a stochastic online model reduction approach for multiscale nonlinear stochastic parabolic PDEs. Multiscales and nonlinearity significantly impact on the computation using traditional FEM in a fine grid. CEM-

GMsFEM and DEIM can substantially improve the computation efficiency. We have carried out the error analysis of CEM-GMsFEM for the nonlinear stochastic PDEs. However, the semi-discrete system is still nonlinear in a high-dimensional space by CEM-GMsFEM. In order to overcome this challenge, we proposed the stochastic online DEIM method, which used the offline mean information and the online trajectory snapshots. The online DEIM significantly reduced the computation complexity for the nonlinear system. By incorporating the stochastic online DEIM with CEM-GMsFEM, we developed a stochastic multiscale model reduction method: Online DEIM-MS. This method showed superiority in prediction compared with Offline DEIM approach. We presented a few numerical examples from the porous media application to show effectiveness of the stochastic online model reduction method.

## REFERENCES

- [1] J. AARNES, Y. EFENDIEV AND L. JIANG, *Mixed multiscale finite element methods using limited global information*, Multiscale Modeling & Simulation, 7(2)(2008), pp.655–676.
- [2] T. ARBOGAST, K. BOYD, *Subgrid upscaling and mixed multiscale finite elements*, SIAM Journal on Numerical Analysis, 44(3)(2006), pp.1150–1171.
- [3] T. ARBOGAST, G. PENICHEVA, M. WHEELER AND I. YOTOV, *A multiscale mortar mixed finite element method*, Multiscale Modeling & Simulation, 6(1)(2007), pp.319–346.
- [4] A. BRAHIM, *Homogenized behavior of two-phase flows in natured reservoirs with uniform fractures distribution*, Transport in Porous Media, 10(1993), pp.43–56.
- [5] H. BESSAIH, Y. EFENDIEV AND R. F. MARIS, *Stochastic homogenization for a diffusion-reaction model*, Discrete & Continuous Dynamical Systems, 39(9)(2019), pp. 5403–5429.
- [6] H. BESSAIH, Y. EFENDIEV AND F. MARIS, *Homogenization of Brinkman flows in heterogeneous dynamic media*, Stochastic Partial Differential Equations: Analysis and Computations, 3(2015), pp.479–505.
- [7] M. BARRAULT, Y. MADAY, N. C. NGUYEN AND A. T. PATERA, *An ‘empirical interpolation’ method: application to efficient reduced-basis discretization of partial differential equations*, Comptes Rendus Mathematique, 339(9)(2004), pp.667–672.
- [8] C.-C. CHU, I.G. GRAHAM, T.-Y. HOU, *A new multiscale finite element method for high-contrast elliptic interface problems*, Mathematics of Computation, 79(272)(2010), pp.1915–1955.
- [9] E. T. CHUNG, Y. EFENDIEV AND T. Y. HOU, *Adaptive multiscale model reduction with generalized multiscale finite element methods*, Journal of Computational Physics, 320(2016), pp.69–95.
- [10] E. T. CHUNG, Y. EFENDIEV AND W. T. LEUNG, *Constraint Energy Minimizing Generalized Multiscale Finite Element Method*, Computer Methods in Applied Mechanics and Engineering, 339(2018), pp.298–319.
- [11] F. CHEN, E. CHUNG AND L. JIANG, *Least-squares mixed generalized multiscale finite element method*, Computer Methods in Applied Mechanics and Engineering, 311(2016), pp.764–787.
- [12] S. CHATURANTABUT, D. C. SORENSEN, *Nonlinear Model Reduction via Discrete Empirical Interpolation*, SIAM Journal on Scientific Computing, 32(5)(2010), pp.2737–2764.
- [13] M. DROHMANN, B. HAASDONK AND M. OHLBERGER, *Reduced basis approximation for nonlinear parametrized evolution equations based on empirical operator interpolation*, SIAM Journal on Scientific Computing, 34(2)(2012), pp.A937–A969.
- [14] J. DUAN, W. WANG, *Effective Dynamics of Stochastic Partial Differential Equations*, Academic Press(2014), Boston.
- [15] W. E, B. ENGQUIST, *Heterogeneous multiscale methods*, Communications in Mathematical Sciences, 1(1)(2003), pp.87–132.
- [16] Y. EFENDIEV, J. GALVIS AND T. HOU, *Generalized multiscale finite element methods*, Journal of Computational Physics, 251(2013), pp.116–135.
- [17] Y. EFENDIEV, J. GALVIS AND X. WU, *Multiscale finite element methods for high-contrast problems using local spectral basis functions*, Journal of Computational Physics, 230(4)(2011), pp.937–955.
- [18] R. G. GORDEEV, *The existence of a periodic solution in a tide dynamics problem*, Journal of Soviet Mathematics, 6(1–4)(1976).
- [19] L. GAWARECKI, V. MANDREKAR, *Stochastic Differential Equations in Infinite Dimensions. with Applications to Stochastic Partial Differential Equations*, Probability and Its Applications(2011), Springer, Berlin, Heidelberg.

- [20] T. HUGHES, G. FEJOO, L. MAZZEI AND J. QUINCY, *The variational multiscale method – a paradigm for computational mechanics*, Computer Methods in Applied Mechanics and Engineering, 166(1-3)(1998), pp.3-24.
- [21] O. ILIEV, R. LAZAROV AND J. WILLEMS, *Variational multiscale finite element method for flows in highly porous media*, Multiscale Modeling & Simulation, 9(4)(2011), pp. 135-1372.
- [22] R. JUANES, *A variational multiscale finite element method for multiphase flow in porous media*, Finite Elements in Analysis and Design, 41(7–8)(2005), pp.763-777.
- [23] P. JENNY, S. LEE, H. TCHELEPI, *Multi-scale finite volume method for elliptic problems in subsurface flow simulation*, Journal of Computational Physics, 187(1)(2003), pp.47-67.
- [24] L. JIANG, Y. EFENDIEV AND G. VICTOR, *Multiscale methods for parabolic equations with continuum spatial scales*, Discrete Contin. Dyn. Syst. Ser. B, 8 (2007), pp. 833–859.
- [25] R. KRUSE, *Strong and Weak Approximation of Semilinear Stochastic Evolution Equations*, Lecture Notes in Mathematics, 2093(2014), Springer International Publishing.
- [26] P. E. KLOEDEN, S. SHOTT, *Linear-implicit strong schemes for Itô-Galerkin approximations of stochastic PDEs*, Journal of Applied Mathematics and Stochastic Analysis, 14(1)(2001), pp.47-53.
- [27] D. KULASIRI, W. VERWOERD, *Stochastic Dynamics: Modeling Solute Transport in Porous Media*, North-Holland Series in Applied Mathematics and Mechanics, 44(2002), North Holland.
- [28] V. K. KALANTAROV, S. ZELIK, *Smooth attractors for the Brinkman–Forchheimer equations with fast growing nonlinearities*, Communications on Pure & Applied Analysis, 11(5)(2012), pp.2037-2054.
- [29] M. LI, E. T. CHUNG AND L. JIANG, *A Constraint energy minimizing generalized multiscale finite element method for parabolic equations*, Multiscale Modeling and Simulation, 17 (3) (2019), pp. 996-1018.
- [30] G. J. LORD, C. E. POWELL AND T. SHARDLOW, *An Introduction to Computational Stochastic PDEs.*, Cambridge Texts in Applied Mathematics(2014), Cambridge University Press, Cambridge.
- [31] G. J. LORD, A. TAMBUE, *Stochastic exponential integrators for the finite element discretization of SPDEs for multiplicative & additive noise*, IMA Journal of Numerical Analysis, 33(2)(2013), pp.515-543.
- [32] A. MALQVIST AND D. PETERSEIM, *Localization of elliptic multiscale problems*, Mathematics of Computation, 83 (290) (2014), pp. 2583-2603.
- [33] J. D. MUKAM, A. TAMBUE, *Strong Convergence Analysis of the Stochastic Exponential Rosenbrock Scheme for the Finite Element Discretization of Semilinear SPDEs Driven by Multiplicative and Additive Noise*, Journal of Scientific Computing, 74(2018), pp.937-978.
- [34] D. A. NIELD, A. BEJAN, *Convection in Porous Media-Forth Edition*, Springer(2013), New York.
- [35] B. ØKSENDAL, *Stochastic Differential Equations: An Introduction with Applications-Fifth Edition*, Springer(2003), Berlin, Heidelberg.
- [36] B. PEHERSTORFER, K. WILLCOX, *Online adaptive model reduction for nonlinear systems via low-rank updates*, SIAM Journal on Scientific Computing, 37(4)(2015), pp.A2123-A2150.
- [37] G. D. PRATO, J. ZABCZYK, *Stochastic Equations in Infinite Dimensions*, Encyclopedia of Mathematics and its Applications(2008), Cambridge University Press, Cambridge.
- [38] S. PESZAT, J. ZABCZYK, *Stochastic Partial Differential Equations with Lévy Noise. An Evolution Equation Approach*, Encyclopedia of Mathematics and Its Applications, 113(2007), Cambridge University Press, Cambridge.
- [39] B. STRAUGHAN, *Stability and Wave Motion in Porous Media*, Applied Mathematical Sciences, 165(2008), Springer, New York.
- [40] A. TAMBUE, J. D. MUKAM, *Magnus-type integrator for non-autonomous SPDEs driven by multiplicative noise*, Discrete & Continuous Dynamical Systems, 40(8)(2020), pp.459-4624.
- [41] M. WHEELER, G. XUE, I. YOTOV, *A multiscale mortar multipoint flux mixed finite element method*, ESAIM: Mathematical Modelling and Numerical Analysis, 46(4)(2012), pp.759-796.
- [42] S. ZHANG, X. GUAN AND L. JIANG, *Convergence analysis of constraint energy minimizing generalized multiscale finite element method for a linear stochastic parabolic partial differential equation driven by additive noises*, Journal of Computational and Applied Mathematics, 389 (2021), Paper No. 113328
- [43] Z. ZHANG, G. E. KARNIADAKIS, *Numerical Method for Stochastic Partial Differential Equations with White Noise*, Applied Mathematical Sciences, 196(2017), Springer International Publishing.